Sediment heterogeneity and mobility in the morphodynamic modelling of gravel-bed braided rivers

Singh, Umesh; Crosato, Alessandra; Giri, Sanjay; Hicks, Murray

DOI
10.1016/j.advwatres.2017.02.005

Publication date
2017

Document Version
Accepted author manuscript

Published in
Advances in Water Resources

Citation (APA)
Singh, U., Crosato, A., Giri, S., & Hicks, M. (2017). Sediment heterogeneity and mobility in the morphodynamic modelling of gravel-bed braided rivers. *Advances in Water Resources*, *104*, 127-144. https://doi.org/10.1016/j.advwatres.2017.02.005

Postprint of Advances in Water Resources
Volume 104, June 2017, Pages 127–144
Link to formal publication (Elsevier): https://doi.org/10.1016/j.advwatres.2017.02.005

Sediment heterogeneity and mobility in the morphodynamic modeling of gravel-bed braided rivers

Umesh Singh [a,b]*, Alessandra Crosato [a,c], Sanjay Giri [d], Murray Hicks [e]

[a] UNESCO-IHE, Westvest 7, 2601 DA Delft, the Netherlands

[b] University of Trento, Department of Civil, Environmental and Mechanical Engineering, via Mesiano 77, 38123 Trento, Italy.

[c] Delft University of Technology, Faculty of Civil Engineering and Geosciences, Stevinweg 1, 2628 CN Delft, the Netherlands.

[d] Deltares, River Engineering & Morphology, Inland Water System, Rotterdamseweg 185, 2629 HD Delft, the Netherlands

[e] National Institute of Water & Atmospheric Research (NIWA), PO Box 8602, 8440 Christchurch, New Zealand

* Corresponding author

Email addresses: umesh.singh@unitn.it (U. Singh), a.crosato@unesco-ihe.org (A. Crosato), sanjay.giri@deltares.nl (S. Giri), murray.hicks@niwa.co.nz (M. Hicks)

ABSTRACT

The effects of sediment heterogeneity and sediment mobility on the morphology of braided rivers are still poorly studied, especially when the partial sediment mobility occurs. Nevertheless, increasing the bed sediment heterogeneity by coarse sediment supply is becoming a common practice in river restoration projects and habitat improvement all over the world. This research provides a step forward in the identification of the effects of sediment sorting on the evolution of sediment bars and braiding geometry of gravel-bed rivers. A two-dimensional morphodynamic model was used to simulate the long-term developments of a hypothetical braided system with discharge regime and morphodynamic parameters derived from the Waimakariri River, New Zealand. Several scenarios, differing in bed sediment heterogeneity and sediment mobility, were considered. The results agree with the tendencies already identified in linear analyses and experimental studies, showing that a larger sediment heterogeneity increases the braiding indes and reduces the bars length and height. The analyses allowed identifying the applicability limits of uniform sediment and variable discharge modelling approaches.

KEYWORDS

Gravel-bed braided rivers, morphodynamic modelling, Delft3D, graded sediment, variable discharge, Meyer Peter and Müller formula

1 INTRODUCTION

Braided rivers are characterized by a dynamic system of diverging and converging channels separated by bars [*Lane*, 1957; *Leopold and Wolman*, 1957; *Miall*, 1977, *Bertoldi et al.*, 2009a]. Gravel bed braided rivers are common in pro-glacial environments [e.g. *Rust*, 1972] and piedmont areas [e.g. *Surian and Rinaldi*, 2003] where the discharge is strongly variable and sediments are heterogeneous. Although gravel-bed braided rivers are valued less for the aesthetic point of view [*Lay et al*, 2013], they have high ecological importance. Within a braided river corridor, a complex and dynamic display of aquatic, amphibian and terrestrial habitat elements are present which allows co-existence of many species within the river corridor [e.g. *Tockner et al*, 2006]. Bars are units which provide terrestrial habbitat within the active river corridor. They also serve as resting places for aviary species whereas vegetated bars form the habitat even for mammals. Shape statistics associated with bars such as shore-line length are used to define interface between aquatic and terrestrial habitats, in ecological models [*Tockner et al,* 2006; *van Der Nat et al*, 2002].

Several human interventions in the past century, such as flow alterations, gravel mining, catchment scale sediment management etc have converted braided reaches into transition or single thread rivers [e.g. *Piegay et al*, 2006; *Surian and Rinaldi*, 2003]. As such, Braided river ecosystems are among the most endangered in the world [*Sadler et al*, 2004]. Flow augmentation, such as flow and flood pulses, [*Bertoldi et al, 2009*; *Tockner et al*, 2000] and coarse sediment supply [*Binder*, 2005; *Liebault et al*, 2008; *Piegay et al*, 2009; *Rinaldi et al, 2009*; *Surian et al*, 2009] are some widely practiced measures to restore and manage gravel bed braided rivers. However, understanding of natural complexity and dynmaics of braided rivers are required for developing their sustainable management schemes [*Ward et al.,* 2001; *Peigay et al, 2004*].

Non-uniform bed material composed of mixtures of gravel and sand render the morphodynamic study of gravel-bed braided rivers even more complex. Most laboratory studies on gravel-bed braided rivers have focused in braiding mechanism [Ashmore, 1982; Ashmore 1990], channel morphology [*Hundey and Ashmore*, 2009; *Kasparak et al*, 2015] and vertical grain sorting during braided channel evolution [*Leduc et al, 2015*]. *Lanzoni and Tubino* [1999] extended the classical linear bar theory by introducing sediment non-uniformity. Their analysis shows that non-uniform sediment results in a reduction of alternate bars amplitude and length. *Lanzoni* [2000a and 2000b] performed several flume experiments on alternate bar development with uniform and non-uniform sediment to verify his previous theoretical work. He observed that sediment sorting indeed causes a reduction of the bar amplitude, but has no consistent effects on bar length. *Teramoto and Tsujimoto* [2006] studied the effects of sediment size heterogeneity of bed materials on short-term development of multiple bars by means of a numerical model and a linear stability analysis. They observed that the bar mode increases if sediment heterogenity increases.

Linear and weakly non-linear analyses describe the initial stages of the river bed development starting from a flat bed (e.g. *Callander* [1969]; *Engelund* [1970]; *Engelund and Skovgaard* [1973]; Parker [1976]; *Seminara and Tubino* [1989]; *Colombini et al.* [1987]; *Schielen, et al.* [1993]). For large width-to depth ratios, the initial stages are characterized by the formation of many small migrating bars, resulting in high braiding intensity. Long-term development are characterized by the decrease of the braiding intensity, which is due to progressive bar merging, resulting in larger and less mobile bars. These developments can be described by fully-non-linear models (e.g. *Enggrob and Tjerry'*s [1999]; *Nicholas* [2013]; *Schuurman et al.,* [2013]), since the non-linear terms in the equations describing the river morphodynamic evolution play a crucial role for bar merging.

To summarize, the effects of sediment heterogeneity is studied on long-term evolution of alternate bars and the effects on braiding intensity is studied only at the initial stage of the bed evolution. So there exists a gap in understanding on what type of effects sediment heterogeneity has on the long-term morphodynamics of bars in gravel-bed braided rivers. Based on the results of previous work, we can expect the long-term morphological evolution of gravel-bed braided rivers to be affected by sediment sorting processes [Powell, 1998]. We can also expect to find important differences depending on whether the bed sediment is always fully mobile (all fractions are mobile) or only partially mobile (only the smaller fractions are mobile), since partial mobility may result in local bed armoring and bar stabilization (e.g. *Hunziker and Jaeggi* [2002]; *Parker* [2007]). Numerical modeling of braided rivers with erodible banks by *Sun et al.,* [2015] shows that bed armoring in the channels close to the banks reduces bank erosion and that higher sediment heterogeneity increases this effects, resulting in narrower channels.

The main objectives of this research were to identify the effects of sediment heteroginity on the evolution of bar charachteristics and braiding degree of gravel-bed braided rivers, for partial and full sediment mobility conditions. We analyzed the effects of sediment sorting by varying the sediment grain size distribution in a hypothetical straight river channel with non-erodible banks by means of a two-dimensional (2D) fully-non-linear morphodynamic model. The model settings are based on the Waimakariri River (Figure 1) near Christchurch (New Zealand) to compare results broadly against a prototype natural river, but without the intention of reproducing the evolution of this river in particular. We carried out the sensitivity analyses between a variable hydrograph and a constant discharge regime and several other model parameters, which allowed us to make important choices on their values and analyze their effects on numerical modelling of gravel-bed braided rivers.

2 MODEL DESCRIPTION

2.1 Delft3D

The numerical model was developed using the physics-based, fully-non-linear, open-source software Delft3D [*www.deltares.nl*]. The model solves the unsteady shallow-water equations with hydrostatic approximation [*Lesser et al.*, 2004] in two or three dimensions (2DH). Flow, sediment transport and bottom updating are computed at small time steps [*Roelvink*, 2006].

Bars in river channels create flow bifurcations and confluences and induce curvature of the streamlines. For this, it is important that the model takes into account the effects of the spiral motion that arises in curved flow [*Mosselman and Le*, 2015]. *Schuurman and Kleinhans* [2011] showed that with a relatively coarse computational grid a 2DH model, with parameterized spiral motion, gives results on the large scale bar pattern statistics that are comparable with the results of a fully 3D model. So, to limit computational time, we used a depth-averaged (2DH) model with a parameterization of two relevant 3D effects of the spiral motion [cf. *Blanckaert et al.*, 2003]: the redistribution of the main flow velocity in transverse direction due to the secondary-flow convection and the correction of the sediment transport direction, which would otherwise coincide with the direction of the depth-averaged flow velocity vector. This approach has already been successfully used to model the morphological behavior of braided rivers by *Jagers* [2003], *Marra* [2008], *Crosato and Saleh* [2011], *Schuurman et al.,* [2013] and the long-term evolution of alternate bars by *Crosato et al.* [2011 and 2012].

The model includes a wetting-drying procedure, for which all cells having water depth smaller than a certain depth (in our case 5 cm) are considered dry. To simulate the widening of channels between bars that become exposed during low water flows, a simple erosion formulation is applied at the margin between wet and dry cells, according to which the model assigns a part of the erosion occurring inside wet cells to the adjacent dry cells [*van der Wegen and Roelvink*, 2008; *Schuurman et al*, 2013].

Non-uniform sediment processes are modeled by: (i) subdividing the sediment mixture into a number of sediment fractions, (ii) applying a transport formulae and a mass conservation equation for each separate fraction, (iii) applying hiding-exposure corrections for the critical shear stress of each fraction, (iv) considering an active transport layer participating in sedimentation and erosion, and (v) considering a book-keeping layer or substratum which has become inactive due to sedimentation [*Mosselman*, 2005; *Sloff and Ottevanger*, 2008] based on *Hirano*'s [1971] model. The use of book-keeping layers [*Sloff et al.*, 2001] allows the model to register the composition of the deposited sediment and makes the model more robust [*Blom*, 2003].

Each fraction is defined by the minimum and the maximum sediment size of the fraction, the model then assumes a log-uniform distribution between the extremes of each fraction, whereas the median diameter represents the fraction in the computation.

To properly simulate sorting processes, we adapted the *Meyer Peter and Müller* (MPM) [1948] formula by including *Parker et al.* [1982] hiding-exposure formulation. The transport of each individual fraction was predicted as follows:

$$q_{s,i} = p_i 8\sqrt{\Delta g D_{50,i}^3}\sqrt{(\mu\theta_i - \xi 0.047)^3} \quad (1)$$

where $q_{s,i}$ is the sediment fraction transport per unit width, p_i is the percentage of occurrence of the ith sediment fraction, $\Delta = (\rho_s - \rho)/\rho$ is the relative sediment density with ρ_s = density of sediment and ρ = density of water, $D_{50,i}$ is the median sediment diameter of the ith sediment fraction, $\mu = (C/C_{90})^{3/2}$ is the ripple factor in which C is the Chezy's roughness, $C_{90} = 18\log_{10}(12h/D_{90})$ corresponds to grain Chezy's coefficient, D_{90} is the 90th percentile grain diameter and *h* is the water depth.

In the adapted MPM formula (Equation 1), $\theta_i = u^2 (C^2 \Delta D_{50,i})^{-1}$ is the Shields number, u is depth-averaged velocity and ξ is Parker et al' s hiding-exposure coefficient:

$$\xi = (D_m / D_{50,i})^{\alpha} \tag{2}$$

where D_m is the mean sediment particle size and α is the Parker et al.'s exponent

Hunziker and Jaeggi [2002] and *Wong and Parker* [2006] reanalyzed data sets used by *Meyer Peter and Müller* [1948], and proposed several modifications. *Hunziker and Jaeggi* [2002] extended the MPM formula to non-uniform sediment, decreased the constant from 8 to 5 and slightly increased the value of the critical Shields number to 0.05 (instead of 0.047). *Wong and Parker* [2006] and *Huang* [2010] found that in most cases the form-drag correction is unnecessary. Wong and Parker re-evaluated the formula by modifying the constant and the value of the critical Shields number to 3.97 and 0.0495, respectively.

Hirano's [1971] single-layer model was used for the conservation of mass of the individual sediment fractions:

$$(1-\varepsilon)\frac{\partial(p_{a,i}\delta)}{\partial t} + (1-\varepsilon)p_{f,i}\frac{\partial z}{\partial t} + Morfac \times \left(\frac{\partial(p_i q_s)}{\partial x} + \frac{\partial(p_i q_s)}{\partial y} \right) = 0 \tag{3}$$

Where ε is the porosity, taken as 40% [J*ansen et al.*, 1979], $p_{a,i}$ is the percentage of occurrence of the ith fraction in the active layer, $p_{f,i}$ is the percentage of occurrence of the ith fraction in the sediment flux between the active and sub-surface layers, p_i is the percentage of occurrence of the ith fraction in the transported material, δ is the active layer thickness and z is elevation of the interface between active and sub-surface layer, *Morfac* is the morphological acceleration

factor used to accelerate long-term morphological development. It is important to note that $p_{f,i}$ is equal to $p_{a,i}$ in conditions of sediment deposition and equal percentage of the ith fraction in the subsurface layer $p_{sl,i}$, so,

$$p_{f,i} = \begin{cases} p_{a,i} & if\ \partial z/\partial t > 0 \\ p_{sl,i} & if\ \partial z/\partial t < 0 \end{cases} \quad (4)$$

The formulation by *Koch and Folkstra* [1980] extended by *Talmon et al.* [1995] was used to model the effect of bed slope on sediment transport direction:

$$\tan\alpha_i = \left(\sin\alpha_t - \frac{1}{f_i}\frac{\partial z_b}{\partial y}\right) \times \left(\cos\alpha_t - \frac{1}{f_i}\frac{\partial z_b}{\partial x}\right)^{-1} \quad (5)$$

Where, α_i is the angle between the transport direction of ith sediment fraction with the depth-averaged flow direction; α_t is the angle between the direction of the near bed flow and the depth averaged flow direction calculated as

$$\tan\alpha_t = -A(u^2 + v^2)^{-1/2} \quad (6)$$

In Equation 4, A is the coefficient weighing the influence of helical flow on the direction of bed shear stress; u and v are the depth-averaged flow velocity, in x and y direction, respectively. In Equation 3, f_i is a dimensionless parameter weighing the influence of the gravity pull along the inclined bed for the ith sediment fraction. It is given by

$$f_i = A_{sh}\theta_i^{B_{sh}}(D_{50,i}/h)^{C_{sh}}(D_{50}/D_{50,i})^{D_{sh}} \quad (7)$$

where Ash, Bsh and Csh and Dsh are calibration parameters. D50/h in the case of uniform sediment is implemented as an anology to a similar parameter for the effect of bedforms, $D_{50}/D_{50,i}$ is implemented to incorporate the effects of hiding and exposure [*Sloff and Mosselman*, 2012].

2.2 THE WAIMAKARIRI RIVER

The Waimakariri originates from the Southern Alps in New Zealand and flows into the Pacific Ocean. In its lower course through the Canterbury plains, the Waimakariri shows a typical braided nature, except at Lower Gorge, where it is constricted by rocky banks. More downstream, the river width is constricted first by terraces in Pleistocene fan deposits and then, after the river has emerged onto its own Holocene fan, by embankments and groins designed to protect the city of Christchurch from flooding [*Hicks et al.*, 2002]. Several kilometers from the coast, the river narrows and undergoes a gravel-sand transition where it encounters the low gradient Holocene coastal plain. A 13 km long reach, belonging to the part that is confined by embankments, is selected as the real river example to our modeling exercise (Figure 1). The upstream end of the reach is located at 43°27'46" latitude and 172°18'51" longitude; the downstream end is located at 43°26'44" latitude and 172°28'56" longitude, at a site known as "Cross-Bank" (after *Griffiths* [1979]). In the selected reach, the river forms two mildly-curved bends (averaged sinuosity 1.1); the river width varies between 600 m and 1,000 m, but it is most often around 900 m. The river width is calculated as the sum of width of individual channels and non-vegetated or sparsely vegetated bars.

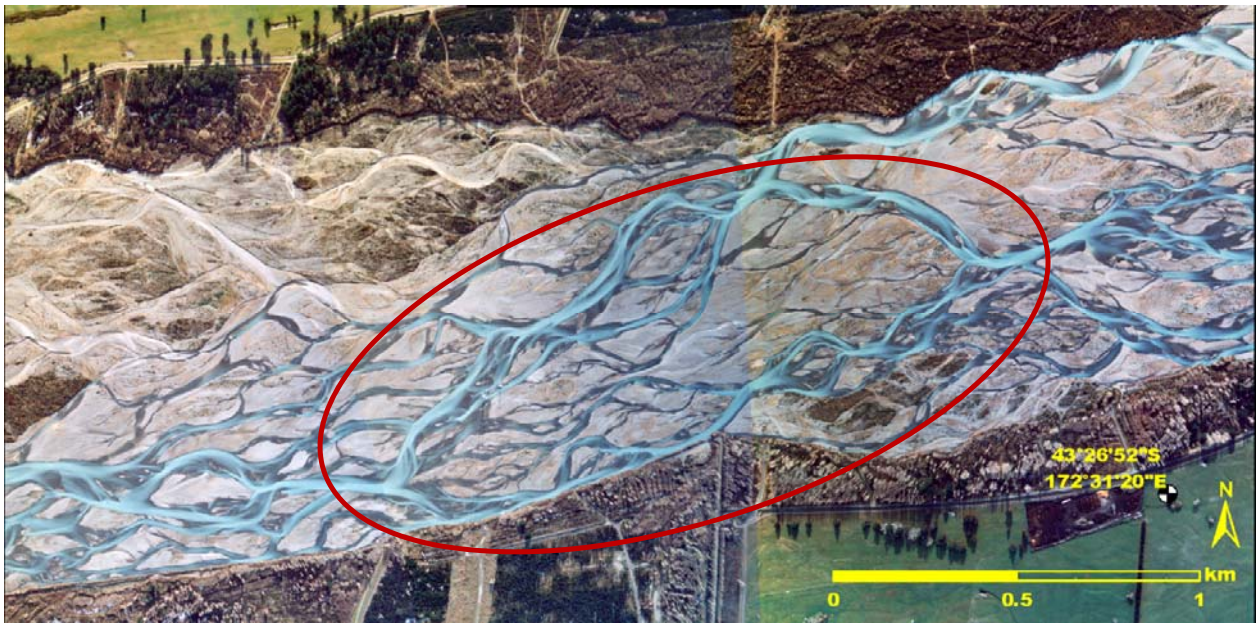

Figure 1. Braided reach of the Waimakariri River near Cross-Bank. Typical compound bar is highlighted by red circle. Flow is from left to right.

All topographic features required for this study were derived from a 5 m resolution DEM, based upon LIDAR and associated image-based bathymetry surveys conducted in July 2003, with root-mean-square error on bed levels of 0.2 to 0.3 m [*Hicks et al.*, 2008]. From the longitudinal bed-level profiles of centre line, right and left banks we obtained an average bed slope of 0.005, which is close to the one previously estimated by *Carson and Griffiths* [1989] (0.0048) for the 30 km upstream of Cross-Bank.

Arial photographs taken during the 2003 survey and Google Earth images show that the bed topography is dominated by large-scale compound bars intersected by a number of small channels and delimited by large morphodynamically-active channels (Figure 1). The reach-averaged bar amplitude, computed as the elevation difference between the top 10% and the smallest 10% detrended values of bed levels is 1.8 m. The reach-averaged length of the compound bars is about 1,000 m. To derive the reach-averaged braiding index of the river, we analyzed 43 cross-sections extracted from DEM at an interval of 250 m. From the measured

bed topography, we counted the bars higher than 0.5 m from the adjacent channel bottom and then derived the corresponding bar mode [*Crosato and Mosselman*, 2009]. The braiding index was found to vary along the reach, ranging between 5 and 18, which is mainly due to channel width variations, the reach-averaged value being equal to approximately 10. In an almost straight, 900 m wide, 1.6 km long sub-reach, the braiding index is 10.7.

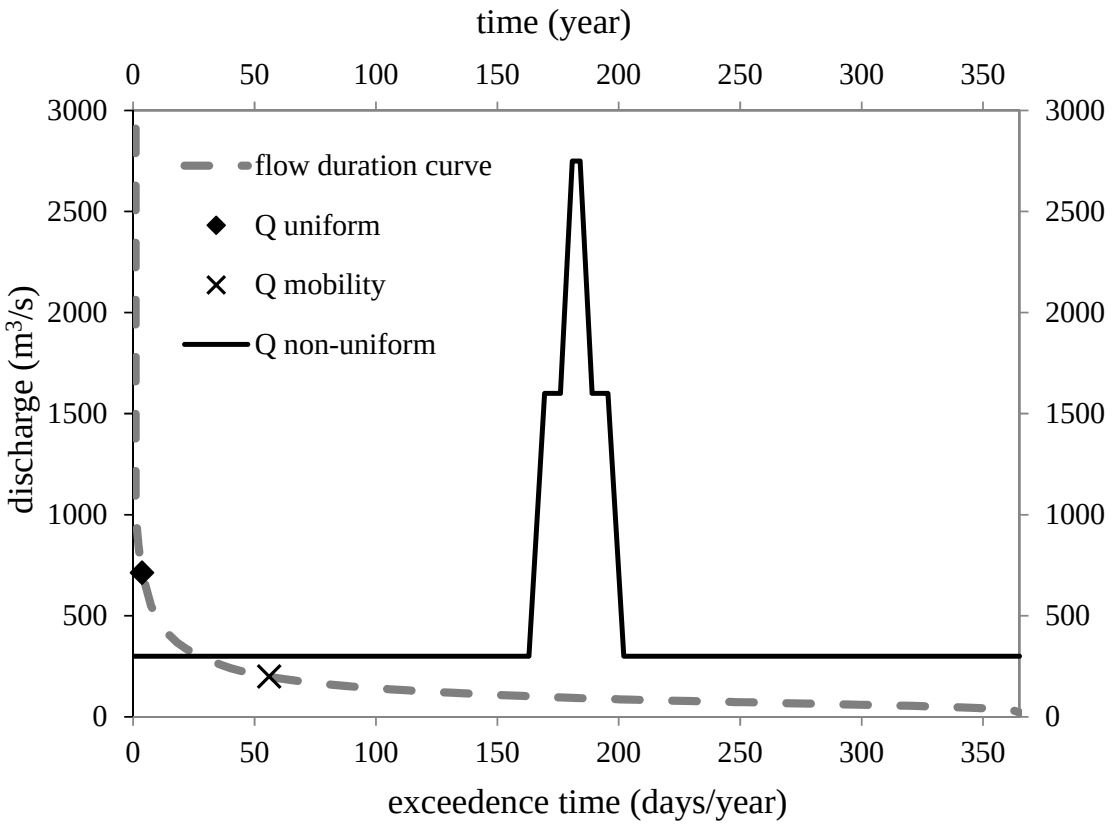

Figure 2. Flow duration curve of the Waimakariri River near State Highway Bridge showing the uniform flow (black diamond) used in the model setup and the non-uniform flow runs (continuous black line) used for sensitivity analysis. The cross indicates the discharge below which sediment mobility becomes negligible at uniform flow conditions.

For this study, we used the discharge time series measured from 1967 to 2006 at the State Highway 1 Bridge, about 11 km downstream from Cross-Bank, without any transformations. This is justified by the absence of significant tributaries in the intervening reach and by minimal

loss of discharge into the gravel bed [*Nicholas*, 2000]. The typical annual hydrograph exhibits two distinct wet seasons in autumn and spring, the mean river flow being 120 m^3/s and the mean annual peak flow 1,520 m^3/s [*Carson and Griffiths*, 1989]. The lowest value of gravel-entraining discharge in the Waimakariri River is 90 m^3/s [*Carson and Griffiths*, 1989], which is exceeded only 50 days per year (Figure 2).

Bed material was sampled at three locations by North Canterbury Catchment Board (NCCB) in 1979. Sediment sizes distribution at the middle part of the reach is shown in Figure 3. In general, the bed material can be classified as poorly sorted (geometric standard deviation 6.75), with median size of 25.4 mm.

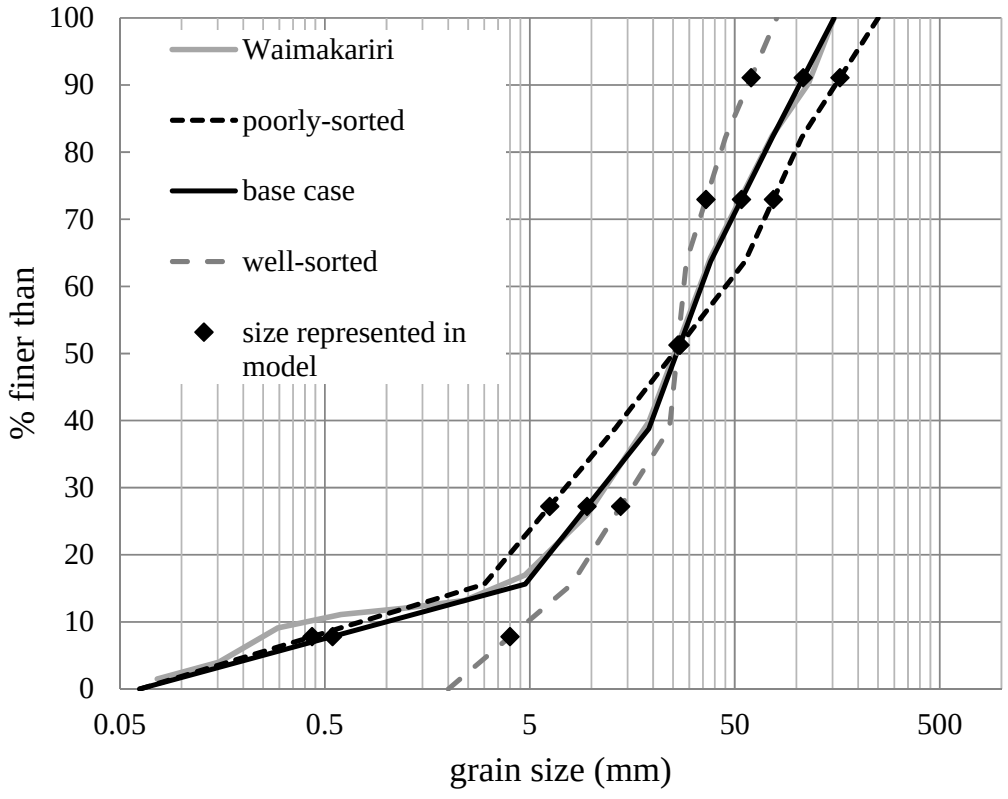

Figure 3. Grain size distributions of Waimakariri River and the different sediment heterogeneity scenarios. Each curve of the scenarios is represented by five fractions. The black dots correspond to the median grain size of each fraction. The uniform sediment scenario is represented by a grain size of 19 mm (average of mean diameters).

2.1 MODEL SETUP

The model domain is a 15,000 m long and 900 m wide straight channel with fixed banks having a longitudinal bed slope of 0.005. *Schuurman and Kleinhans* [2011] show that the large-scale statistics of the bar pattern are independent of computational grid size, but a fine grid describes the shape of compound bars better than a coarse grid. In the attempt to accommodate accuracy of the results with the necessity to restrain computational time, the grid was made by rectangular grid cells 10 m long in transverse direction and 20 m long in longitudinal direction, which resulted in 90 cells in the transverse direction. Model stability was assured by a computational time-step of 3 seconds.

A Manning's coefficient equal to 0.031 $m^{1/3}/s$ (assuming a dimensionless conversion factor k = 1) was derived based on direct measurements of discharge, water levels, wetted area, perimeter and longitudinal slope of a 4 km-long part of the selected reach by *Hicks et al.* [2002]. From this, our model computed the equivalent Chézy's coefficient as $C = (h^{1/6})/n$, where C is Chezy's coefficient, h is the local flow depth and n is Manning's coefficient, at every time step and for every grid cell. In this way, the value of Chézy's coefficient becomes larger (smaller flow resistance) as the water depth increases. The diffusion due to 2D turbulence was specified by a constant horizontal eddy viscosity parameter [*Lesser et al.*, 2004], a value of 1 m^2/s was used based on previous experience from 2D modeling of the Dutch Rhine River branches (e.g. *Kleinhans et al.* [2008]).

Carson and Griffiths [1989] predicted the long-term gravel transport rate of the Waimakariri River near the reference area reasonably well using the standard MPM formula. For this, we used the original formulation, without taking into account suggested adjustments [*Huang*, 2010; *Hunziker and Jaeggi*, 2002; *Wong and Parker*, 2006]. Parker et al.'s exponent with the value of 0.75 was used to model hiding and exposure effect (Equation 2). This approach was chosen after comparison with several other approaches, because it provided sediment transport

rate results that best resembled the ones of *Wilcock and Crowe* [2003]'s formula (not implemented in the numerical model). This surface-based formula was used as a reference because it had been derived experimentally for graded sediments in conditions close to real rivers and validated on the field with some modifications by *Gaeuman, et al.* [2009].

Both active and book-keeping layers were given a thickness of 1.25 m, corresponding to approximately the reach-averaged half maximum bar amplitude (calculated as the elevation difference between the highest point of the bar and deepest point in the channel). *Schuurman et al.* [2013] showed that the morphological evolution of braided rivers were marginally affected by the morphological acceleration factor that is imposed to speed up morphodynamic computations. So, a morphological acceleration factor (morfac) equal to 25 was used to accelerate long-term morphological evolution (Equation 3).

To model the effects of bed slope on sediment transport direction, we considered to use the values recommended by *Sloff and Mosselman* [2012], *Mosselman* [2005] and *Talmon* [1995] based upon the modeling of real rivers: $A_{sh} = 9$, $B_{sh} = 0.5$, $C_{sh} = 0.3$ and $D_{sh} = 0$ (Equation 7). D_{sh} parameter takes into account the effects of hiding and exposure on the effects of bed slope on sediment transport direction which is poorly understood. We only implemented the hiding and exposure effects in the sediment transport predictor (Section 2.1) and neglected its effects here by imposing $D_{sh} = 0$, to reduce the number of the calibration parameters.

The discharge of 700 m^3/s was provided at the inlet. The normal water level corresponding to the inlet discharge and initial bed slope of the channel was provided as the outlet boundary. An equilibrium sediment transport corresponding to the local hydraulic condition close to upstream boundary was prescribed at the inlet.

The simulations were carried out for each scenario starting from an almost flat bed. A small initial bed level undulation was imposed to trigger morphodynamic instability and quickly obtain bar formation. At the end of the computations, the system is supposed to have reached

a "dynamic equilibrium". In this study, the dynamic equilibrium is characterized by a braiding index that is constant. Considering this, after having performed some preliminary computational tests, the duration of the simulations was set to either 10 years (full mobility) or 14 years (partial sediment mobility scenarios). Since the Waimakariri River is morphodynamically active only 50 days per year, this was also the duration of the computations representing one single year. Considering that we used a value of the morphological factor, morfac, equal to 25, 10 years of morphological evolution were covered by 20 computational days and 14 years by 28 days.

Several scenarios were defined based on sediment mixture characteristics and sediment mobility conditions to assess the effects of sediment size heterogeneity on the morphology of braided rivers. Altering the size heterogeneity of the bed sediment, we defined four scenarios differing in bed sediment composition. The sediment grain size distribution of the Waimakariri River represents the base-case scenario. Then two granulometric curves with the same median diameter, D_{50} (27 mm), but different size ranges were generated. The largest sediment sizes were increased and the smallest sizes decreased, although maintaining the smallest limit of 0.0625 mm, in the curve representing more poorly sorted sediment, with higher size heterogeneity than the base case (Table 1, poorly sorted scenarios, and Figure 3). The largest sediment sizes were decreased and the smallest sizes increased for the well sorted sediment scenarios, with less size heterogeneity than the base-case (Table 2, well sorted scenarios, and Figure 3). The geometric standard deviation of poorly sorted scenarios, base case and well sorted scenarios are 6.88, 5.38 and 2.35 respectively. Finally, the study also includes the scenarios with uniform sediment (no size heterogeneity), having particle diameter equal to the average geometric mean diameter D_m (19 mm) of the mixtures.

Table 1. Subdivision in 5 sediment fractions. Mobility of sediment fractions of P1, P0 and P2 (partial mobility) and F1, F0 and F2 (full mobility) scenarios at the start of the computations with a (virtually) flat channel bed and uniform flow of 700 m^3/s.

sed. fraction	D_{min} (mm)	D_{max} (mm)	percentage of volume (%)	mean size D_m (mm)	median size D_{50} (mm)	D_{max}/D_{min}	$\mu\theta$	ξ	*partial mobility*			*full mobility*		
									θ_i	$(\mu\theta)/\theta_i$	b	θ_i	$(\mu\theta)/\theta_i$	b
poorly sorted scenarios P1/F1 (highest heterogeneity)														
1	0.0625	3	15.62	0.76	0.4	48.0	3.67	37.0	1.74	2.1	6	0.74	4.95	4
2	3	13	23.18	6.82	6	4.3	0.25	5.0	0.23	1.1	40	0.10	2.54	5
3	13	56	24.91	29.44	27	4.3	0.06	1.7	0.08	0.8	-	0.03	1.76	7
4	56	106	18.5	78.36	77	1.9	0.02	0.8	0.04	0.6	-	0.02	1.36	11
5	106	250	17.79	167.83	163	2.4	0.01	0.4	0.02	0.5	-	0.01	1.13	27
base-case scenarios P0/F0 (Waimakariri River)														
1	0.0625	4.75	15.62	1	0.5	76.0	2.5	24.7	1.16	2.2	6	0.49	5.07	4
2	4.75	19.05	23.18	10	10	4.0	0.14	2.9	0.14	1.1	59	0.06	2.48	5
3	19.05	38.10	24.91	27	27	2.0	0.05	1.3	0.06	0.8	-	0.03	1.91	6
4	38.10	76.20	18.50	55	54	2.0	0.03	0.8	0.04	0.7	-	0.02	1.61	8
5	76.20	152.40	17.79	110	108	2.0	0.01	0.5	0.02	0.6	-	0.01	1.35	12
well-sorted scenarios P2/ F2 (smallest heterogeneity)														
1	2.0000	8.00	15.62	4.3	4	4.0	0.28	4.3	0.20	1.4	11	0.09	3.23	4
2	8.00	24.00	23.18	14.6	14	3.0	0.08	1.7	0.18	1.0	477	0.03	2.36	5
3	24.00	29.00	24.91	26.4	26	1.2	0.04	1.1	0.05	0.9	-	0.02	2.01	6
4	29.00	45.00	18.5	36.4	36	1.6	0.03	0.8	0.04	0.8	-	0.02	1.86	6
5	45.00	80.00	17.79	60.8	60	1.8	0.02	0.6	0.03	0.7	-	0.01	1.64	8
uniform sediment scenario P3/F3 (no heterogeneity)														
1	19	19	100	19	19	1	0.08	1	0.047	1.78	7	0.020	4	4

We obtained the computational scenarios P0, P1, P2 and P3 in which P0 represents the base-case scenario; P1 (highest size heterogeneity) is the scenario with (more) poorly sorted sediment if compared to P0; P2 (lowest heterogeneity) is the scenario with well sorted sediment if compared to P0. Because not all sediment fractions are always mobile, these scenarios represent partial mobility conditions. Finally, P3 is the uniform sediment scenario, for which the sediment is necessarily (fully) mobile.

For these scenarios, the sediment transport rate was computed using the MPM formula, which refers to the mean sediment diameter of the mixture, with its standard critical threshold value of 0.047 (Equation 1). The hiding-exposure coefficient for each individual fraction, ξ, was computed using Equation 2. We checked the sediment mobility of each fraction, considering that a sediment fraction is mobile if:

$$\left(\mu\theta / \theta_i\right) \geq 1 \text{ with } \theta_i = \xi \times 0.047 \tag{8}$$

Where μ = ripple factor and θ = Shields number.

We computed also the non-linearity of sediment transport with respect to flow velocity as [*Crosato and Mosselman*, 2009]:

$$b = 3\mu\theta\left(\mu\theta - 0.047\right)^{-1} \tag{9}$$

This parameter rapidly increases if the sediment is close to the conditions of initiation of motion. Table 1 shows that at the beginning of the simulations, with a flat channel-bed and uniform flow distribution, only the finest two fractions were mobile as well as uniform sediment of simulation P3. Based on the large values of *b*, the second sediment fraction was close to initiation of motion.

To study the effects of full sediment mobility versus partial sediment mobility on the morphological evolution, we defined another set of four computational scenarios with reduced threshold of sediment motion (0.02 instead of 0.047) in Equations 1, 8 and 9 maintaining all other parameters unchanged. In this way, we obtained comparable runs.

The full mobility conditions are represented by scenarios F0, F1, F2 and F3 which are the counterparts of scenarios P0, P1, P2 and P3, respectively. The uniform sediment scenarios, F3 and P3, are in fact both fully mobile. Their difference lies basically in the threshold used for initiation of motion and in their sediment transport rates. Table 1 provides the sediment characteristics of all sediment scenarios and the mobility check of each fraction for these scenarios.

2.3 Sensitivity Analyses

The results of morphodynamic simulations of gravel-bed braided rivers are strongly affected by a number of model parameters and discharge regime. Considering previous experiences, we analyzed the effects of varying the values of these important parameters by means of sensitivity analyses.

The Waimakiriri River discharge is strongly variable, as in every natural gravel-bed braided system. Generally in this type of rivers, high flows occur infrequently and for short periods of time. The Waimakariri is morphodynamically active only for about 50 days per year, when the discharge is larger than 90 m^3/s [*Carson and Griffiths*, 1989]. To avoid strong discharge variations causing model instability, we designed the computational yearly discharge hydrograph based upon the flow duration curve. The schematized hydrograph is then repeated for the number of years that characterize the duration of the simulation. This type of approach has been already successfully used for long-term morphodynamic modeling (e.g. *Yossef and Sloff* [2012]). In the computational variable-discharge hydrograph (Figure 2), the minimum

value of the discharge (300 m^3/s) corresponds to an averaged low flow and the maximum value (2,750 m^3/s) corresponds to an averaged flow event occurring for one day per year.

For variable discharge, the value of morfac used in our model decreases as the value of the discharge increases so that the highest value of morfac (200) is applied for the smallest value of the discharge (300 m^3/s), for which the sediment transport rate is very small, and no acceleration is applied to the highest discharge (morfac = 1), since during peak flow conditions the sediment transport rate is high and the morphological changes are relatively fast.

A number of scientists [e.g. *Leopold and Wolman*, 1957; *Fredsøe* 1978; *Hey and Thorne*, 1986; *van den Berg*, 1995; *Parker et al.*, 2007] suggested using the bankfull discharge or the mean annual flood [eg. *Antropovskiy, 1972; Bray, 1982*] to represent the formative conditions of a river. We selected the value of the constant discharge based on the best fit between the Waimakariri River morphology and the results of our model. The discharge of 700 m^3/s results in the best fit and can be considered to represent the "formative discharge".

Gravity diverts bed load along the downslope direction [e.g. *Koch and Flokstra*, 1980], which decreases bar amplitudes and produces sediment sorting (summarized by *Powell* [1998]). *Schuurman et al.* [2013] showed that the morphological evolution of braided rivers is affected by the effects of transverse bed slope parameterization on bed load direction. These effects are especially important for bar formation (see also *Mosselman and Le*, [2015]).

We included the effects of bed slope parameterization on the bed load direction using the formulation by *Koch and Folkstra* [1980] extended by *Talmon et al.* [1995] (Equation 3). This equation requires calibration based on the optimization of the following parameters: A_{sh}, B_{sh}, C_{sh} and D_{sh} (Equation 5). Increasing the value of A_{sh} directly lowers the bed slope effects and this is also obtained by decreasing the value of C_{sh}. However, unlike A_{sh} (parameter studied already by *Schuurman et al.*, [2013]), C_{sh} imposes different bed slope effects for each sediment fraction [*Sloff and Mosselman,* 2012]. Dealing with graded sediment and focusing on the

effects of sediment size heterogeneity, we decided to investigate the effects of varying C_{sh}. This coefficient weighs the effects of bed slope for different sediment fractions, through the sediment size to local water depth ratio. D_{50}/h ratio is larger on bar tops and smaller in channels. Since $C_{sh} < 1$, increasing D_{50}/h results in smaller values of f_i (Equation 5) and increasing effects of bed slope on sediment transport direction (Equation 3). We performed three runs simulating the long-term morphological evolution starting from an almost flat bed with different values of this parameter: 0.2, 0.3 and 0.4. We considered the base-case scenario under full mobility conditions with $A_{sh} = 9$ and $B_{sh} = 0.5$ [*Talmon et al*., 1995], whereas we omitted the contribution of sediment sorting on the effects of bed slope by imposing $D_{sh} = 0$. The value of Ash and Bsh is commonly used as 1.5 and 0.5 respectively if Csh and Dsh are ignored [e.g. *Sloff and Mosselman*, 2012]

Sloff and Mosselman [2012] showed that the thickness of the active bed layer is important for the simulation of both sediment sorting and bed topography. *Hirano*'s [1971] method requires the definition of the thickness of the layer of sediment that is actively participating in the sediment transport process. The sediment underneath comes into action in cases of scouring. The thickness of the active layer, which is kept constant during the computations, plays a sensitive role in the performance of the model [*Blom,* 2008; *Sloff and Ottevanger*, 2008]. Hirano assumed the active layer thickness to be equal to the maximum grain size. Later, *Armanini and Di Silvio* [1988], *Parker* [1991] and *Ribberink* [1987] suggested using half the amplitude of dunes on the river bed, whereas *Blom* [2008] suggested using the entire dune amplitude. This approach is confirmed by *Sloff and Ottevanger* [2008], *Mosselman* [2012] and *Sloff and Mosselman* [2012], who show that in modeling real rivers (Dutch Rhine branches), the active layer thickness requires much higher values than half the dune amplitude.

Although a few studies indicate the presence of dune-like structures in the channels of gravel bed rivers [e.g. *Dinehart*, 1992], there is no evidence of dune formation in the reference river.

Moreover, our study focuses on the reworking of bars. For this, an active layer equal to half of or the entire bar amplitude may result in more realistic results. To study the effects of active layer thicknesses on river braiding, we carried out a sensitivity analysis. We performed several morphological simulations starting from an almost flat bed for the base-case scenario under full mobility and partial mobility conditions. The smallest thickness of 0.2 m corresponds to three times D_{90}. The thickness of 1.25 m is close to half the maximum bar amplitude, defined as the difference in level between the highest bar top and deepest channel bed level. We also investigated the thicknesses of 2, 5 and 10 meters to study the effects of large active layer thickness. We included relatively large thickness of 10 m to investigate the case in which the active layer corresponds to the entire alluvial bed. The sub-surface was divided into a number of book-keeping layers with the same thickness as the active layer to make the model more robust.

2.4 Analysis Methods

To compare different scenarios and detect temporal trends, we analyzed the bed topography distribution at specific times and the temporal evolution of reach-averaged cross-sectional sediment transport rate, braiding index, reach-averaged bar amplitude and bar length. We also analyzed the median grain size sediment distribution to understand the effects of sediment sorting processes on the channel evolution. A 10 km reach was chosen for the analysis after removing 2.5 km reach each at the upstream and downstream boundary to eliminate boundary effects. *Egozi and* Ash*more* [2008] state that the sample-reach length should be at least 10 times the channel width at the channel forming discharge. Their criteria are based upon a laboratory experiment but serves as the basic criteria for rivers as well. Since, width of the river in the model is 900 m we consider that 10 km reach is sufficient for the analysis.

Considering that the bar merging process results in progressive reduction of braiding index, we assumed that the river bed topography can be considered as fully-developed when the braiding index reaches a stable value. For this, the temporal evolution of the braiding index and reach averaged cross-sectional sediment transport rate were used as a measure to establish whether morphodynamic equilibrium is achieved.

Egozi and Ashmore [2008)] provide a list of indices that are used to represent the index of river braiding. The "channel count index" appears as a promising one, since it is easily quantifiable and comparatively less sensitive to river-stage effects. *Bertoldi, et al.* [2009b], however, suggested counting only the channels which are morphologically active, which results in a stage-dependent "active braiding index". The "bar mode"-m- [*Engelund and Skovgaard*, 1973] is another effective parameter to define the river braiding intensity. This is the number of parallel alternate-bar rows that are needed to reproduce the topographic pattern of the river channel: $m = 1$ corresponds to a channel with alternate bars, typical of meandering rivers; $m = 2$ corresponds to a channel with central bars, typical of rivers in transition between meandering and braiding; and $m > 2$ corresponds to a channel with multiple bars, typical of braided rivers. Bar mode is similar to the channel count index, but is derived by counting the number of faces of bars wetted by a channel rather than the channels alone [*Kleinhans and van den Berg*, 2011].

The braiding index is here represented by the bar mode, m. It is derived using the method developed by *Schuurman et al.,* [2013], which consists of counting the number of parallel channels crossing the river cross-sections and then computing the reach-averaged value. Channels are identified by a bed level below the cross-sectional averaged one. This method includes both active and inactive channels. The bar mode is then computed from the number of channels, since the number of channels in the cross-section increases by 0.5 if m increases by 1 [e.g. *Crosato and Mosselman*, 2009].

The bed topography of braided rivers consists of a complex network of mid-channel bars and ephemeral channels. Bars are submerged during high flow and exposed during low flows. In this context, there is no clear definition or threshold level to distinguish bars from channels.

Hypsometric curves have been mostly used to represent the fluvial forms and processes within a river basin [e.g. *Willgoose and Hancock*, 1998] or to characterize and evaluate the development of the morphological features in estuaries and tidal inlets [e.g. *Marciano et al.,* 2005; *Wang et al.,* 2002]. The use of hypsometric curves is not common in river morphodynamics, but they appear as a suitable tool to assess the complex topography of braided rivers in statistical terms. The advantage of using this method is that it does not require a threshold limit to define bars and channels, whereas it shows the extension of areas above or below certain levels. Different bar/channel distributions, as well as different bar amplitudes, result in different hypsometric curves. So, the hypsometric curves can be effectively used to compare the topographical characteristics of river reaches and modeling results. We derived the hypsometric curve from the bed topography after detrending by initial bed slope. In our hypsometric curves, the detrended bed elevation is given in the *y*-axis, where it is represented by the distance between the bed and a reference plane. The percentage of area having a smaller value is given in the *x*-axis. Negative values are characteristic of the low areas (channels) and positive value belong to the high areas (bars).

To represent the reach-averaged bar amplitude, we adopted the method by *Schuurman et al.,* [2013], in which the bar top is defined as the highest 10 % and the channel deepest point as the lowest 10 % of detrended bed elevation (in the hypsometric curves the levels corresponding to 10 and 90 % of area, respectively). The reach-averaged difference between these two levels is then assumed to be the representative bar amplitude.

To compute the reach-averaged bar length, bars were assumed to be represented by all areas having water depth smaller than half the reach-averaged water depth at a discharge of 700 m^3/s.

After having mapped all bars, we measured their length. Since at every moment in time several bars of different size are present, we computed the percentage of surface occupied by all bars having the same length which was then assumed to be their weight. The weighted average was then used as representative reach-averaged bar length.

3 RESULTS

3.1 Main results

Figure 4 shows evolution of water depth distribution in P0 scenario. Deeper parts (blue) represent channels and shallow parts (white) represent bars. Starting from the near flatbed topography, 0 years, several small amplitude bars appeared in the river bed at the initial stage of the morphological evolution, 0.25 years. Smaller bars then merged together and formed larger bars as the development progressed (2.5 years). Bars continued to merge and become larger and flow concentrated in few deep channels (10 years). Similar morphological evolution trends were observed in other partial mobility scenarios (P1, P2 and P3) and full mobility scenarios (F1, F0 and F3). Figure 5 shows water depth distribution after 10 years of morphological evolution. Full-mobility eventually resulted in much deeper channels and in bed topographies that are highly irregular (some irregularities might be produced by local model instability), whereas partial mobility resulted in more realistic channel-bar patterns (compared to the Waimakariri River, Figure 1).

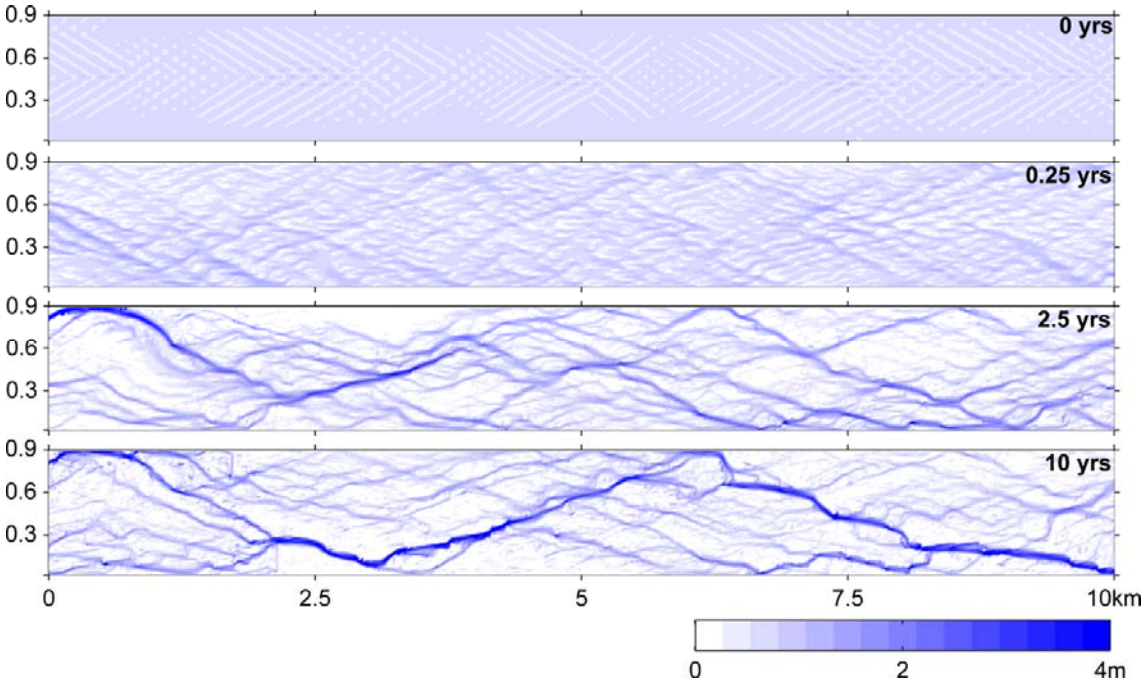

Figure 4 Temporal evolution of water depth distribution in base case scenario (P0). Flow is from left to right.

Figure 6 shows median sediment grain size (D_{50}) distribution during the morphological evolution in the partial mobility scenario-P0 (left) and the full mobility scenario-F0 (right). In the P0 scenario, larger D_{50} were observed in the channels whereas finer D_{50} on top of the bars. D_{50} increased in channel bed as the morphological evolution progressed which denoted the coarsening of the channel bed and possibility of channel bed armoring. Similar trends were observed in P1 and P2 scenarios as well (Figure 7). P1 and P2 scenarios had the largest and smallest sediment size representing coarse part of their sediment size distribution curve respectively (Figure 3 and Table 1). So, the largest and smallest D_{50} was observed in the channels of scenario P1 and P2 respectively.

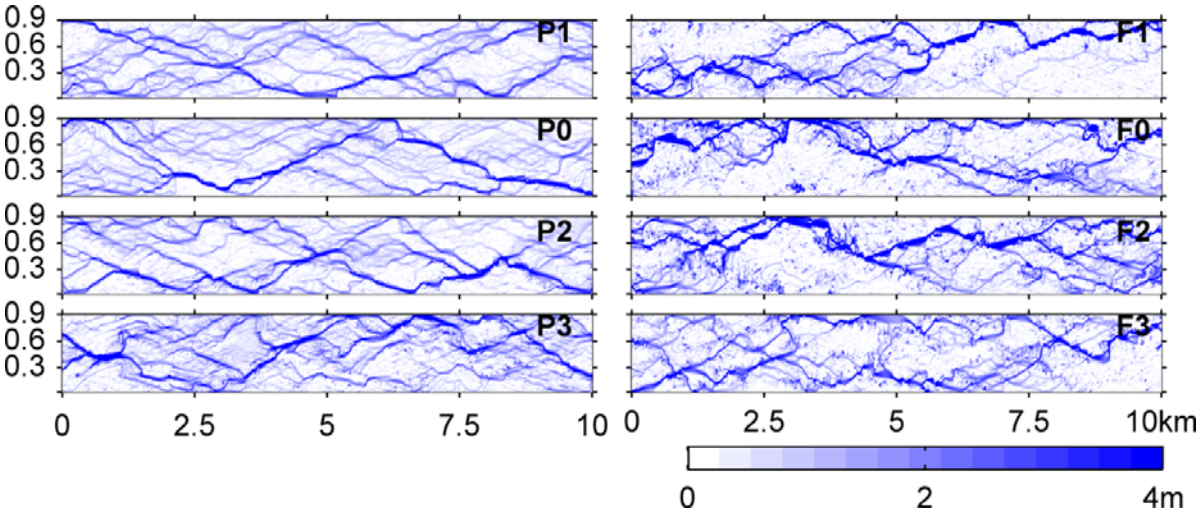

Figure 5 Water depth distribution after 10 years of morphological evolution for the full-mobility scenarios (right column) and for the partial-mobility scenarios (left column). Constant discharge equal to 700 m^3/s. Colour bar: water depths in meters. Flow is from left to right. P1/F1: poorly sorted ; P0/F0 : base case; P2/F2 : well sorted and P3/F3: uniform sediment scenarios.

Unlike in P0 scenario, D_{50} distribution did not show any consistent pattern among channels and bars in F0 scenario. However, larger D_{50} were observed in some parts of the deeper channels. Similar trends were also observed in F1 and F2 scenarios (Figure 7). Since F1 scenario had highest sediment heterogeneity and the F2 scenario had the lowest sediment heterogeneity, the variation in D_{50} size distribution was also observed highest in the F1 and lowest in the F2 scenario.

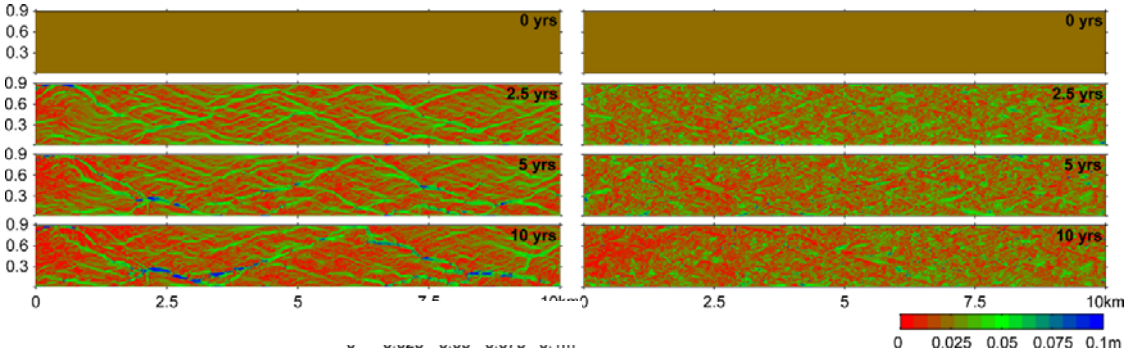

Figure 6 Median grain size distribution during morphological evolution for the full-mobility scenarios (right column) and for the partial-mobility scenarios (left column). Flow is from left to right.

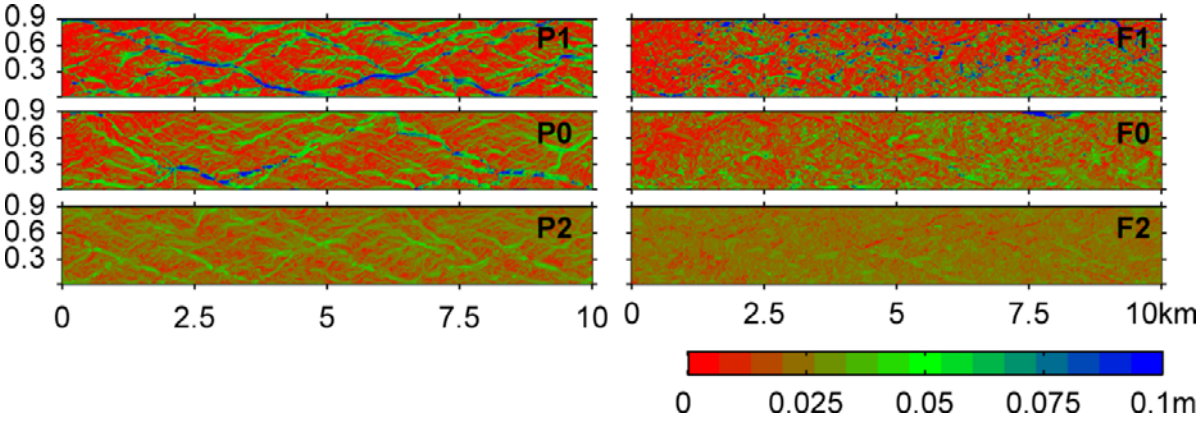

Figure 7 Medium sediment grain size (D_{50}) distribution after 10 years of morphological evolution for the full-mobility scenarios (right column) and for the partial-mobility scenarios (left column). Flow is from left to right. P1/F1: poorly sorted; P0/F0 : base case; P2/F2 : well sorted.

The temporal evolution of the reach-averaged sediment transport rate is shown in Figure 8 (partial mobility scenarios) and Figure 9 (full mobility scenarios) shows the transport rates of each sediment fraction, as well as the total sediment transport rates. As expected, reduction of the threshold for sediment motion in the full mobility scenarios results in higher sediment transport rates and relatively higher contributions of the coarser fractions to the total transport. Note that P0 and P1 have similar sediment transport rates (Figure 9) and that the smallest size fractions are responsible for the highest bed material loads. The uniform sediment scenario results in the lowest rates.

Oscillations of the sediment transport rates are typical features of braided rivers [*Ashmore,* 1991] in which channel excavation and consequent flow concentration result in increased sediment transport rates. Comparing the evolution of the sediment transport rates with the evolution of the braiding indices (Figure 10 a, dotted line), we can observe that the stabilization of the sediment transport rate does not represent the equilibrium, since the development and

redistribution of the bars and channels also occur when the total sediment transport rates is relatively constant.

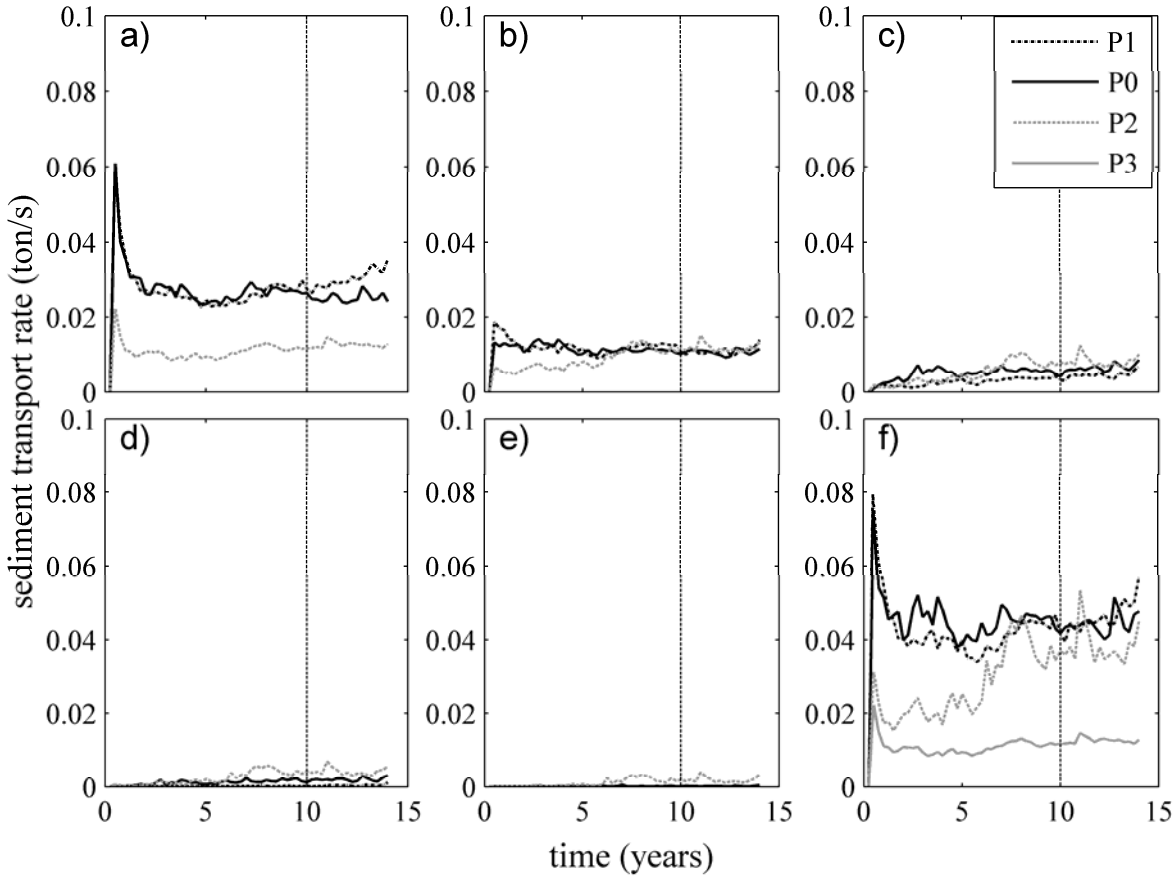

Figure 8. Temporal evolution of the reach-averaged cross-sectional sediment transport rate of a) sediment fraction 1 (finest), b) fraction 2, c) fraction 3, d) fraction 4, e) fraction 5 (coarsest fraction) and f) sum of all fractions for the sediment heterogeneity scenarios P1, P0, P2 and P3 (partial mobility). P1: poorly sorted; P0 : base case; P2 : well sorted and P3: uniform sediment scenarios.

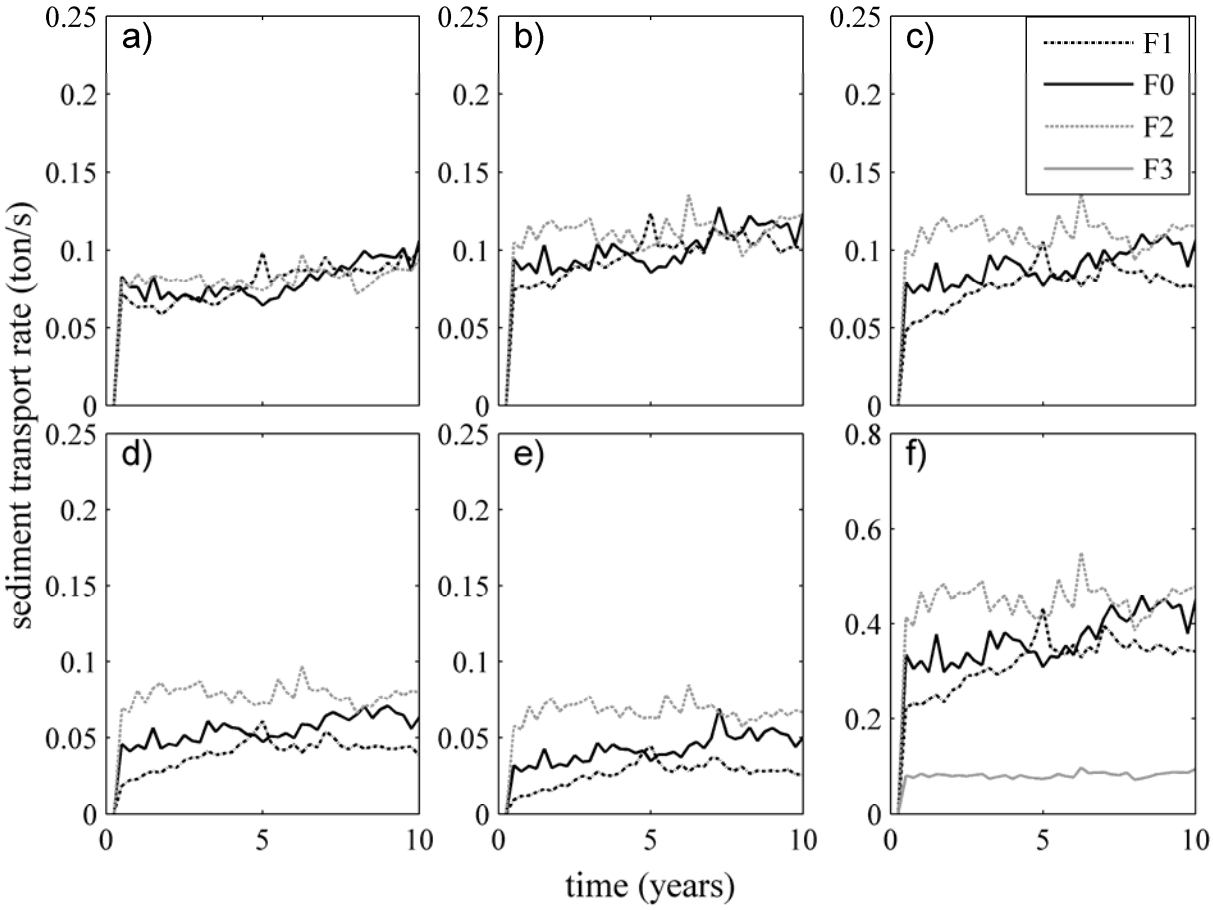

Figure 9. Temporal evolution of the reach-averaged cross-sectional transport rate of a) sediment fraction 1 (finest), b) fraction 2, c) fraction 3, d) fraction 4, e) fraction 5 (coarsest fraction) and f) sum of all fractions for the sediment heterogeneity scenarios F1, F0, F2 and F3 (full mobility). F1: poorly sorted; F0: base case; F2: well sorted and F3: uniform sediment scenarios.

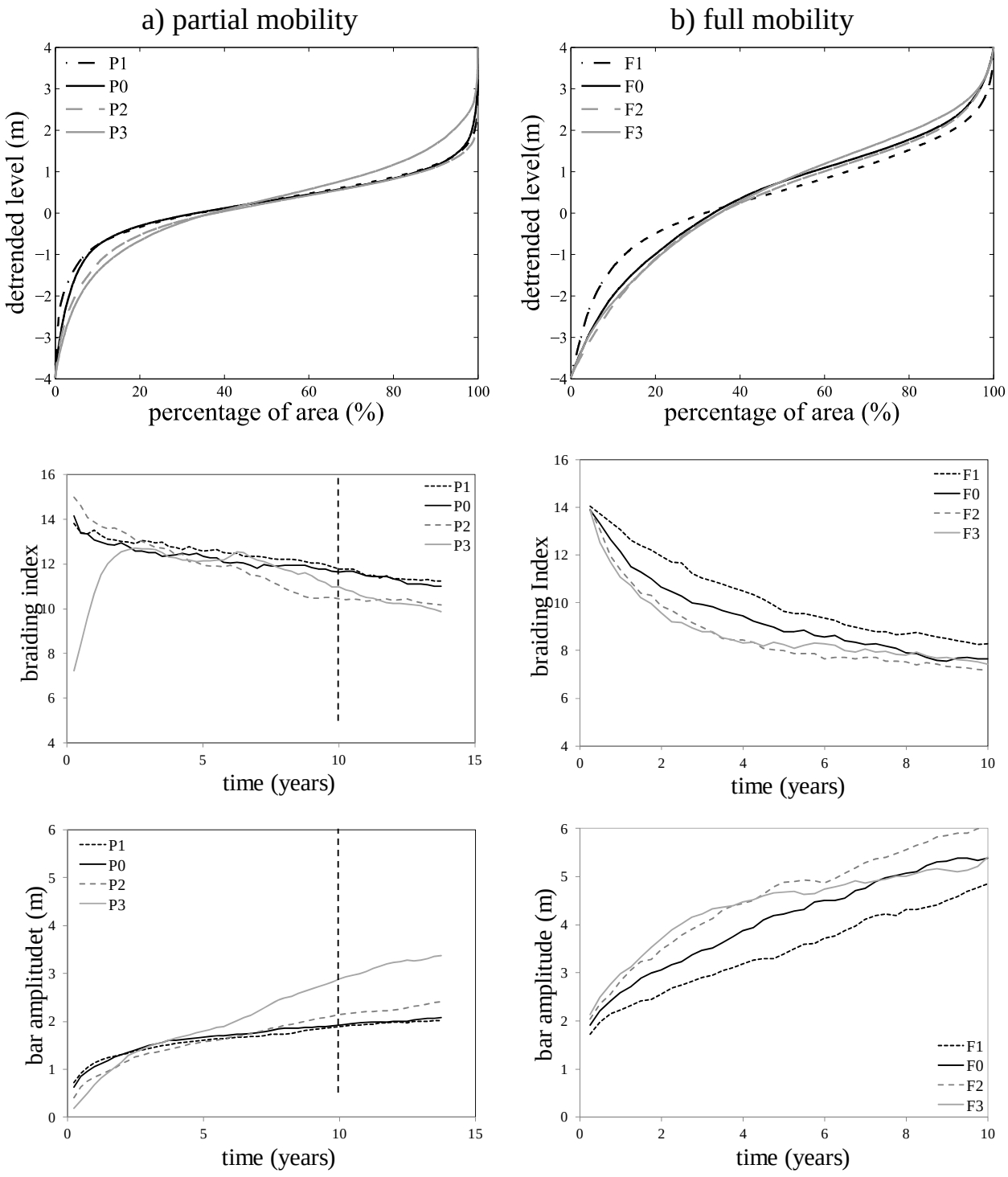

Figure 10. Top to bottom: hypsometric curves at the end of the computations; temporal evolution of braiding index; and temporal evolution of bar amplitude, computed as the elevation difference between the top 10% and the smallest 10% detrended values of bed levels. a): partial mobility scenarios (P1, P0, P2 and P3) and b): full mobility scenarios (F1, F0, F2 and F3). P1/F1: poorly sorted ; P0/F0 : base case; P2/F2 : well sorted and P3/F3: uniform sediment scenarios.

Comparing the partial-mobility scenarios, we observed that uniform sediment (P3) showed an initial temporal lag in the bed topography development with respect to the heterogeneous sediment cases, which is caused by the much lower sediment transport rates (Figure 8). A time lag could be observed also for the bar length development (Figure 11 a). High growth rates of bar length occurred in the latest phases of the development, to the point that uniform sediment ended up with the longest bars. Similar results were obtained for the averaged bar amplitude (Figure 10, column a): in the early stages of the development, the bar amplitude increased with the sediment heterogeneity, but later this trend reversed, with uniform sediment (P3) resulting in the highest bars. Summarizing, uniform sediment eventually produced the largest bars (2,000 m long with an amplitude of 3.2 m), resulting in the most unrealistic morphology if compared to the reference sub-reach of the Waimakariri River, whose bars are, on average, 1,000 m long and 1.8 m high. The excessive bar development can be explained by the fact that uniform sediment is always characterized by full mobility (one single mobile fraction), whereas the other scenarios always had one or more sediment fractions that are not mobile. Scenarios P1 (poorly sorted) and P0 (base-case) always resulted in similar developments, with final braiding indices gradually stabilizing near the value of 12. These two scenarios produced the most realistic results: a reach-averaged bar amplitude of 1.9 m and a bar length close to 1,000 m (Figure 11a). Note that these two scenarios differ in sediment size heterogeneity, being P1 more heterogeneous than P0, but behave similarly, because the sediment fraction 5 was not mobile (Figure 8e). Based on braiding index and bar amplitude, as well as total sediment transport, the two scenarios seemed to have reached a condition of morphodynamic equilibrium at the end of the computations, i.e. after 10 years. The bar length (Figure 11a), however, was still slightly growing, which is a sign of progressive on-going bar merging.

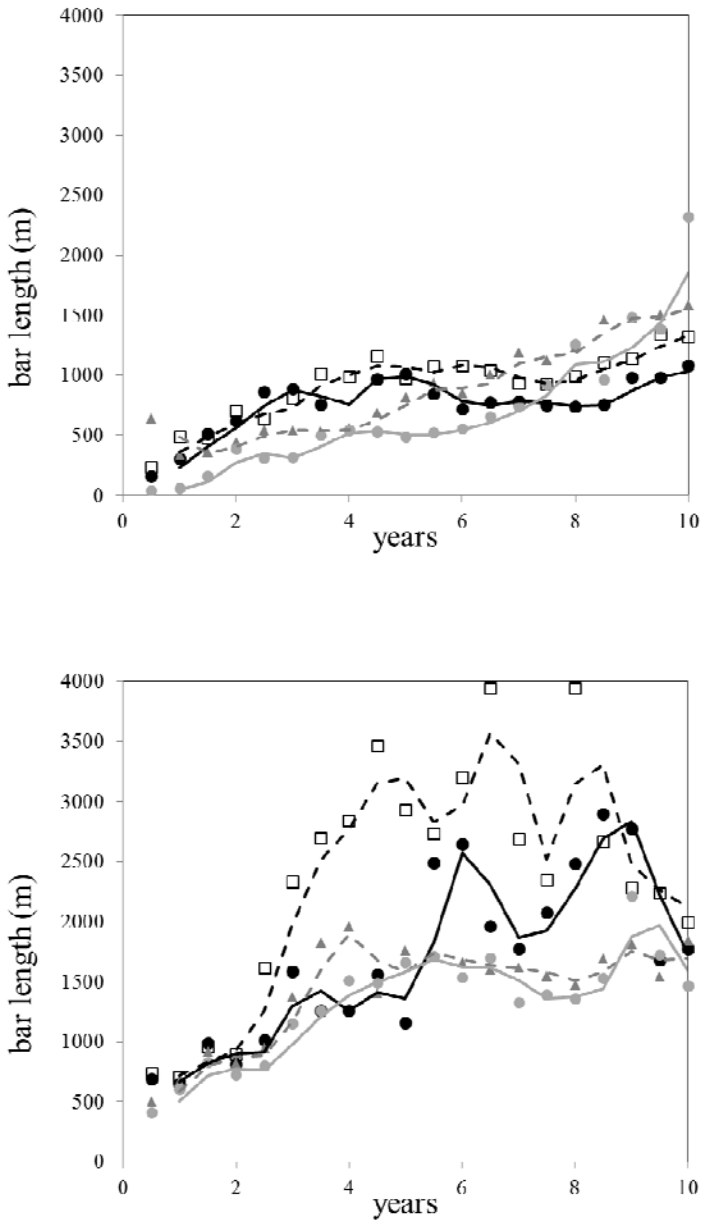

Figure 11. Temporal evolution of bar length. a) partial mobility scenarios P1 (open square), P0 (black filled circle), P2 (grey filled triangle) and P3 and b) full mobility scenarios F1 (open square), F0 (black filled circle), F2 (grey filled triangle) and F3 (grey filled circle).

In the full-mobility scenarios we can observe that the poorly-sorted sediment (highest heterogeneity), F1, resulted in the lowest bars and the highest braiding index, whereas well-sorted sediment (smallest heterogeneity), F2, produced the highest bars and the smallest braiding index. The results of the base-case scenario, F0, lay in between (Figure 10, column b). Surprisingly, also uniform sediment, F3,

produced values close to the base-case scenario. Hiding-exposure effects, not present with uniform sediment, might be responsible for this, since they produced increased mobility of the coarsest fractions and decreased mobility of the smallest fractions in the other non-uniform sediment scenarios. The temporal variations in bar length are more confused (Figure 11b), but in general the most poorly sorted sediment (highest heterogeneity), F1, resulted in the longest bars and the scenarios with the low sediment heterogeneity, F2 and F3, in the shortest. However, at the end of the computations all sediment scenarios resulted in similar bar lengths (1.5-2.0 km).

In general, as expected, the full mobility conditions resulted in more intense morphodynamic variations than the partial mobility conditions. This is reflected in the smaller final braiding indices, an indication of more advanced bar merging. Full mobility conditions produced results that differ considerably from the measured ones: larger bar amplitudes: 4.8 - 6.0 m against the measured 1.8 m, as well as bar lengths: 2,000 m against 1,000 m. Uniform sediment, scenario F3, produced results which fall between the results of the heterogeneous scenarios. Similar results were obtained for uniform sediment also by *Nicholas* [2013].

3.2 Model Sensitivity

Bars and braiding properties were found to be highly sensitive to the transverse bed slope effects parameterization. The results of the sensitivity analysis showed that higher values of C_{sh}, producing relatively larger bed slope effects, developed larger and deeper channels, lower braiding index, and higher bars (Figure 12). This could be observed by analyzing the hypsometric curves of the bed topography after 10 years of morphological evolution (Figure 12a). Increasing the C_{sh} value from 0.3 to 0.4 decreased the braiding index up to 23% and increased the bar amplitude up to 23% during the morphological evolution. Similarly, lower values of C_{sh}, producing relatively smaller bed slope effect, lead to smaller channels, lower bars and more braiding. Reducing the value of C_{sh} from 0.3 to 0.2 increased the braiding index up to 35% and decreased the bar amplitude up to 19%.

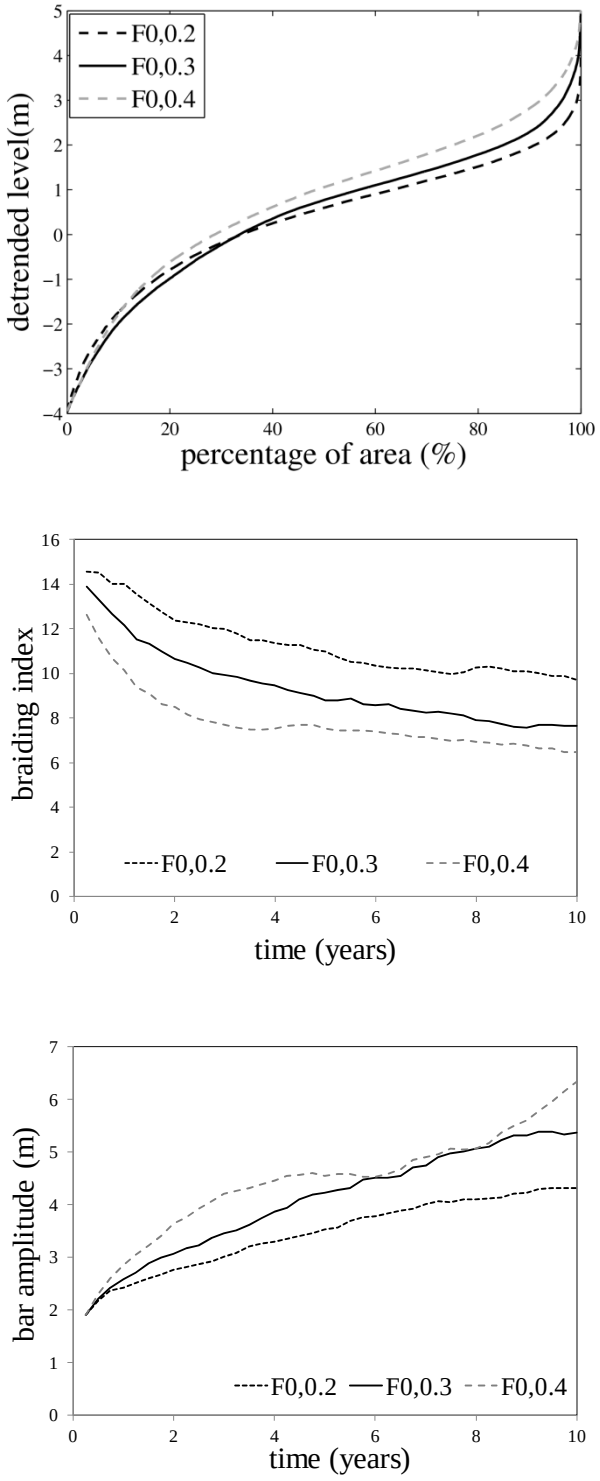

Figure 12. a) hypsometric curves of bed topography after 10 years of morphological evolution for C_{sh} = 0.02; 0.03 and 0.04, b) temporal evolution of braiding index and c) temporal evolution of bar amplitude obtained with the different values of coefficient C_{sh}. The computations refer to the base-case scenario with full mobility conditions.

Figure 13 shows final hypsometric curves, the temporal evolution of braiding index and bar amplitude resulting from different values of the active layer thickness. The results showed that full and partial mobility conditions led to different morphological behaviors. In general, for the same active layer thickness full mobility conditions resulted in deeper channels and higher bars, but smaller braiding indices.

The volume of sediment fraction available for erosion from the channel bed is directly proportional the active layer thickness. In the case of thin active layers (0.2 m), the volume of fine sediment fraction is less, so they were eroded immediately from the channel bed. Since, the coarser sediment fractions were not mobile in partial mobility scenario they were left in the channel bed leading to formation of armor layer which resulted in strongly retarded bed development. This is observable from the hypsometric curves.

The volume of fine sediment fractions increases if the active layer thickness is increased. The larger amount of fine sediment fractions increased the bed mobility thus increasing the morphological evolution at the initial phase. As the morphological evolution progressed, bars merged and flow was concentrated in the channels, which increased the mobility of the larger sediment fractions in the channel bed thus leading to a more complex morphology, with significantly higher braiding indices and bar amplitudes.

Since all of the sediment fractions were mobile with full sediment mobility scenarios, the results of the morphological simulations were less dependent on the active layer thickness. Nevertheless, the 0.2 m thickness generally resulted in the smallest braiding indices and lowest bars and the 10 m thickness in the highest braiding indices and bars.

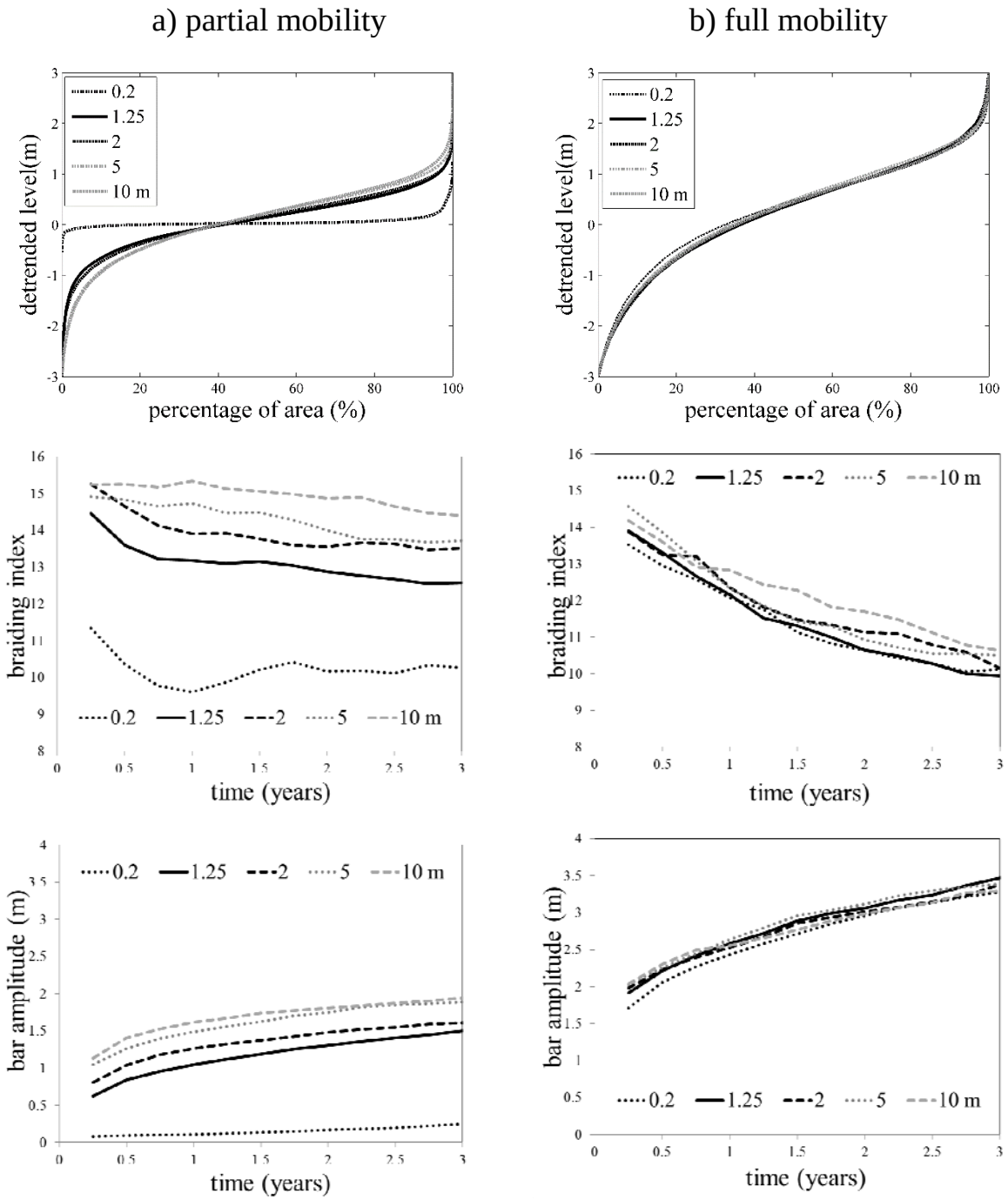

Figure 13. Temporal evolution of channel bed topography (from top to bottom): hypsometric curves, braiding index and bar amplitude obtained for different values of the active layer thickness in case of a) partial sediment mobility and b) full sediment mobility. The values 0.2 to 10 correspond to the different thicknesses of the active layer in meters.

Figure 14 shows the hypsometric curves of bed topography, braiding index and bar amplitude compared between those obtained from the variable-discharge hydrograph and a constant discharge of 700 m^3/s. With variable discharge, an almost equilibrium braiding index, reaching the value of 8 is achieved after 8-10 years (Figure 14b). However, at the end of the computations the bar amplitude is still growing, although at a very small rate (Figure 14c). Approaching equilibrium, effects of the single discharge peaks become negligible for both braiding index and bar amplitude.

Comparison between the computed hypsometric curves and the measured one (Waimakariri River) shows that the constant discharge scenario produces the most realistic distribution of bed topography. The braiding indices obtained with the variable discharge hydrograph (BI = 8) and the constant discharge regime (BI = 12) show that the constant discharge results in a braiding index that is closer to the measured one, the braiding index in the 900 m wide straight part of the Waimakariri River being BI = 10.7. The constant discharge scenario also results in the most realistic (averaged) bar amplitude: 1.9 m, against the 4 m obtained with variable discharge, the reference measured one being 1.54 m.

The water depth distributions obtained at the end of the computations are shown in Figure 15. It is possible to observe that the constant discharge produced a denser and more realistic network of channels than the variable discharge regime (compare to Figure 1, showing the Waimakariri River).

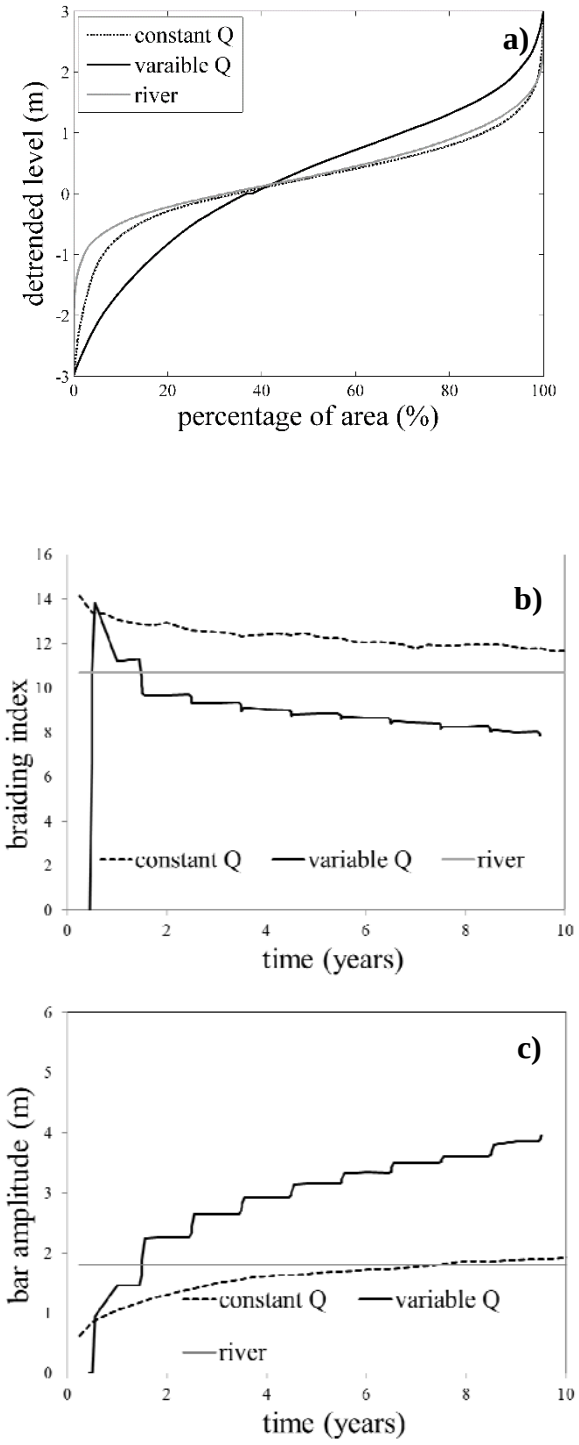

Figure 14. a) hypsometric curves at the end of the computations for constant and variable discharge and hypsometric curve of the Waimakariri River, b) temporal evolution of braiding index obtained with constant and variable discharge (base-case) and c) temporal evolution of bar amplitude, computed as the difference between the top 10% and the smallest 10% detrended values of bed levels.

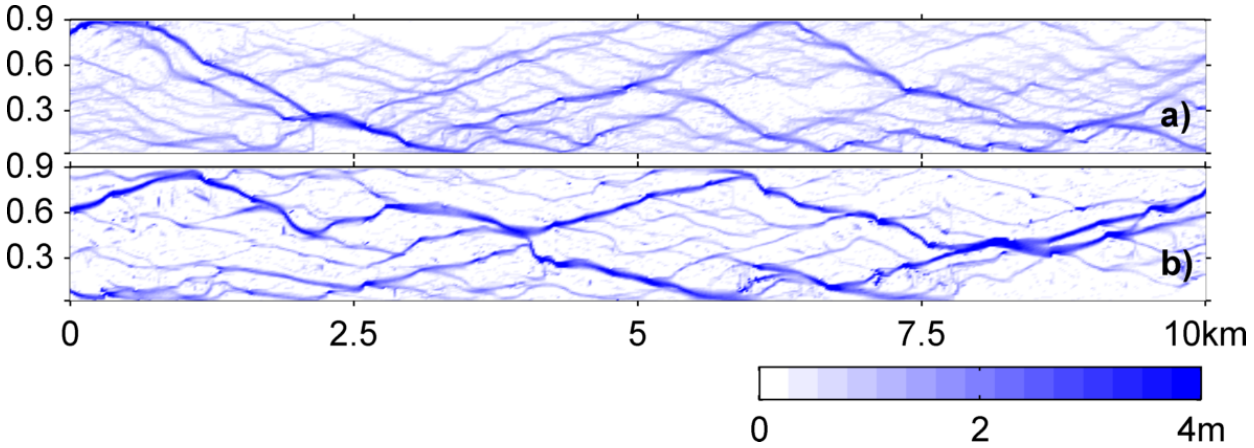

Figure 15. Water depth distribution at the end of the computations showing the network of channels: a) with constant discharge (700 m^3/s) and b) with variable discharge at the same flow conditions (700 m^3/s). Base-case sediment scenario. Flow direction from left to right.

8 DISCUSSION

We carried out a numerical analysis in this study using a fully non-linear morphodynamic model Delft3D. The numerical model was set up with the morphodynamic variables obtained from the Waimakariri River, New Zealand, without the intention to reproduce any specific river. The numerical runs were carried out in a straight channel with fixed banks starting from almost flat bed (containing small perturbations to trigger bar development). The morphological evolution of bar was described by the appearance of several small amplitude bars in the river bed at the initial stage followed by bar merging to form larger bars at the later stage of the development, confirming the general evolution trend reported in the literature [*Fujita*, 1989; *Enggrob and Tjerry*, 1999; *Nicholas et al*, 2013; *Schuurman et al*; 2013]. The trend of evolution of braiding index and bar height approaching to a stable value indicate that the morphological evolution is approaching to an equilibrium condition.

The morphodynamic evolution of river bars depend on the sediment transport boundary condition at the inlet. *Mendoza et al* [2016] show that in a finite domain, the sediment boundary conditions which allow periodicity or fluctuations at the upstream inlet result in more dynamic and realistic bar morphology. *Nicholas et al* [2013] used periodic fluctuation of river bed at the upstream boundary, to mimic

propagation of bar at the inlet, such that more dynamic bar configuration is achieved during the morphological evolution of braided channel. An equilibrium sediment transport corresponding to the local hydraulic condition close to upstream boundary was prescribed at the inlet in this study. It allowed to impose fluctuations compared to constant sediment feed at the inlet. However imposing re-circulating sediment transport boundary condition, which takes into account sediment transport fluctuation due to propagation of bar, at the inlet may result in more dynamic bars than those observed in this study.

This study shows that braiding index increases and bar amplitude decreases if the sediment heterogeneity is increased. Interventions affecting the river bed sediment, like gravel augmentation, alter both the sediment heterogeneity and the median grain size. Assuming full sediment mobility, *Crosato and Mosselman* [2009] show that larger median diameters, reflecting in larger sediment transport non-linearity (Equation 9), result in increased braiding indices (bar modes) and reduced bars (wave) lengths. These additional effects should be taken into account when planning any interventions that alter the bed sediment.

We analyzed the effects of transverse bed slope effect parametrization on the morphological evolution of braided river by altering value of C_{sh}. Braiding intensity and bar amplitude were observed to be affected by the value of C_{sh}. Braiding intensity decreased with increase in transverse bed slope effects (higher C_{sh}), which are in agreement with Figure 18 of *Schuurman et al*. [2013], who performed a similar analysis, by altering the coefficient A_{sh} with a constant discharge and full sediment mobility. They made analysis with active braiding index which only takes into account the channels transporting sediment. The transverse bed slope effect relation implemented by *Schuurman et al* [2013] does not include the C_{sh} parameter.

The bar amplitude increased if the bed slope effect increased. *Schuurman et al* [2013] observed opposite trend in the bar height. A lower braiding index corresponds to a smaller number of deeper channels and

higher bars than a higher braiding index. The smallest braiding index is found for the highest bed slope effects, which explains why the bar amplitude is the highest for this value of C_{sh}.

Transverse slope effect parameters is chosen as calibrating parameter to adjust patterns of bars and pools in numerical modelling application on real rivers [*Sloff and Mosselman*, 2012]. We do not aim to model individual bars and channels of any specific river reach in this study. So the value of Csh = 0.3, chosen based on modelling experience of real rivers [e.g. Talmon et al, 1995], is reasonable for this study. *Nicholas et al* [2013] argue that generic understanding of morphological evolution of bars and channels can be obtained from the numerical model without precisely calibrating the parameters of the transverse bed slope effects.

Thickness of active layer strongly affected the morphological development in the partial mobility scenario. Based on the results, we can observe that the active layer thickness must be much larger than the largest grain size to model the morphological evolution of gravel-bed braided river at partial mobility conditions . Since bars are reworked during morphological development by braiding processes, *Leduc et al* [2015] recommend to use active layer thickness with respect to bar amplitude, in the morphological study of braided channels. So, active layer thickness of about half of the maximum bar amplitude was used for the numerical modelling in this study.

The comparison between model simulations and measured data shows that, contrary to expectations, the constant-discharge approach leads to results that are much more realistic than the variable-discharge approach. The reasons for this might lie in the use of the MPM sediment transport formula. This formula is not suitable for cases with high flow velocity (as during discharge peaks), since high flow velocities result in Shields parameters that are much larger than the critical value for sediment motion ($\theta \gg \theta_{crit}$ with θ_{crit} = 0.047 if the ripple factor is assumed equal to 1) (Mosselman [2005], p.78; Siviglia and Crosato [2016]). In this case, according to the MPM formula, the sediment transport capacity becomes

independent of grain size, which is not realistic. Secondly, MPM predicts at high mobility that the relative amount or concentration of sediment in motion does not increase if bed shear stress increases. Third, MPM predicts at high mobility that narrowing of the river bed leads to steeper slopes, contrary to common observation.

The formula should therefore always be applied within its applicability range, in compliance with the conditions of the laboratory experiments under which it was derived: $\omega_s / u_* > 1$, D_m >0.4 mm and $\mu\theta < 0.2$, with D_m = mean sediment grain size, ω_S = fall velocity of sediment, μ = ripple factor (in this study μ =1), and $u_* = u\sqrt{g / C^2}$ = bed shear velocity [*Meyer Peter and Müller*, 1948].

During computations, the Shields parameter exceeds the value of 0.2 in both runs with variable and constant discharge. In the simulation with constant discharge, the value of 0.2 is exceeded only locally and sporadically, inside the deepest channels (link to supplementary material 1). Instead, in the simulations with variable discharge, peak conditions systematically result in excessive Shields parameters, reaching the value of 0.5, in a large area of the computational domain (link to supplementary material 2).

9 CONCLUSIONS

We carried out a numerical analysis to study the effects of sediment heterogeneity on the long-term morphological evolution of gravel-bed braided systems. To obtain realistic simulations, the numerical model was set up with the morphodynamic variables obtained from the Waikariri River, New Zealand.

Larger sediment heterogeneity resulted in increased braiding indices, confirming the findings of *Teramoto and Tsujimoto* [2006], as well as reduced bar size (amplitude and length), confirming the findings of *Lanzoni and Tubino* [1999]. With full sediment mobility, however, the highest sediment

heterogeneity produces the longest bars. *Lanzoni* [2000b] had contradictory experimental results on the effects of sediment heterogeneity on bar length. A possible explanation could be that these effects depend on sediment mobility, since bars become shorter with partial sediment mobility and longer with full sediment mobility, if the sediment heterogeneity increases. It is important to note that *Lanzoni and Tubino* [1999] and *Lanzoni* [2000b] focused on alternate bars. This work shows that their conclusions are valid also for multiple bars, even after the bar merging process.

The results of this study indicate that uniform sediment cannot be an acceptable assumption to study the long-term response of natural gravel-bed braided rivers, because these rivers are generally characterized by partial sediment mobility. In this case, uniform sediment is found to produce an unrealistic bed topography, characterized by bars that are too long and too high with respect to those observed in nature. Moreover, due to the relatively small sediment transport rates resulting in delayed bed adaptations, the uniform sediment scenario requires longer computational times to reach the conditions of morphodynamic equilibrium.

Instead, the uniform sediment approach appears acceptable in case of full-mobility conditions. However, even in this case, the short-term and mid-term evolution, governed by the bar merging process, might present important differences. Full mobility conditions are mostly found in sand-bed rivers or in very large gravel-bed braided rivers, like the Congo at Kinshasa [*Peters*, 1978]. The long-term morphological response of braided rivers like the Yamuna, in Bangladesh, characterized by sandy (full-mobile) bed material, can therefore be studied with the assumption of uniform sediment (*Ashworth et al* [2000]; *Jagers* [2003]).

In this study, contrary to expectations, the "formative" constant discharge has produced results that are much more realistic than the variable discharge, compared to the morphology of the Waimakariri River. The reason could be found in the use of the *Meyer Peter and Müller* formula [1948] at all flow conditions. This transport formula is not suitable if the value of the Shields parameter falls outside its applicability

range [*Mosselman,* 2005; Siviglia and Crosato, 2016]. Given the lack of sediment transport formulas covering all coarse sediment transport conditions, from incipient motion (low discharges) to extreme mobility (peak flows), a solution to this problem could be the application of different formulas during the morphological computations, selecting the most appropriated one based on the instant value of Shields parameter or bed shear stress.

ACKNOWLEDGEMENTS

The authors would like to express their gratitude to Filip Schuurman and Maarten Kleinhans who allowed them using their codes to compute braiding indes and bar characteristics. The authors thank Arthur Mynett and Erik Mosselman for their valuable guidance and availability, as well as Astrid Blom, Ton Hoitink, Ralph Schielen and Howard Southgate for their enthusiastic participation at discussions. The Environment Canterbury who kindly supplied the LIDAR and flow data for the Waimakariri River. Hicks's input was supported by the New Zealand Ministry for Science and Innovation through Contract C01X0308. Singh's input was funded by the Netherlands Fellowship Program (NFP) and NUFFIC.

REFERENCES

Armanini, A., and G. Di Silvio (1988), A one-dimensional model for the transport of a sediment mixture in non-equilibrium conditions, Journal of Hydraulic Research, 26(3), 275-292, doi: 10.1080/00221688809499212.

Ashmore, P. E. (1982), Laboratory modelling of gravel braided stream morphology, Earth Surf. Process. Landforms, 7(3), 201–225, doi:10.1002/esp.3290070301.

Ashmore, P. (1991), Channel Morphology and Bed Load Pulses in Braided, Gravel-Bed Streams, Geogr. Ann. Ser. A, Phys. Geogr., 73(1), 37, doi:10.2307/521212.

Antropovskiy, V.I. (1972), Quantitative criteria of channel macroforms, Soviet Hydrology, 477-484.

Ashworth, P.J., Best , J.L.. Roden, J.E., Bristow, C.S.and G.J. Klaassen (2000), Morphological evolution and dynamics of a large, sand braid-bar, Jamuna River, Bangladesh. Sedimentology, 47: 533–555. doi: 10.1046/j.1365-3091.2000.00305.x.

Bertoldi, W., A. Gurnell, N. Surian, K. Tockner, L. Zanoni, L. Ziliani, and G. Zolezzi (2009a), Understanding reference processes: linkages between river flows, sediment dynamics and vegetated landforms along the Tagliamento River, Italy, River Research and Applications, 25(5), 501-516, doi:10.1002/rra.1233.

Bertoldi, W., L. Zanoni, and M. Tubino (2009b), Planform dynamics of braided streams, Earth Surface Processes and Landforms, 34(4), 547-557, doi: 10.1002/esp.1755.

Bertoldi, W., L. Zanoni, and M. Tubino (2010), Assessment of morphological changes induced by flow and flood pulses in a gravel bed braided river: The Tagliamento River (Italy), Geomorphology, 114(3), 348–360, doi:10.1016/j.geomorph.2009.07.017.

Binder, W. (2004), Restoration of rivers and floodplains in Bavaria, in 3rd European Conference on RIver Restoration, pp. 17–21, Zagreb.

Blanckaert, K., L. Glasson, H.R.A. Jagers, and C.J. Sloff (2003), Quasi-3D simulation of flow in sharp open-channel bends with equilibrium bed topography, in River, Coastal and Estuarine Morphodynamics: RCEM 2003, 1-5 Sept. 2003, Barcelona, Spain, eds. A. Sánchez-Arcilla & Bateman A., IAHR, Vol. I, pp. 652-663.

Blom, A. (2003), A vertical sorting model of rivers with non-uniform sediment and dunes, Phd Thesis, University of Twente, Netherlands.

Blom, A. (2008), Different approaches to handling vertical and streamwise sorting in modeling river morphodynamics, Water Resour. Res., 44(3), W03415, doi: 10.1029/2006WR005474.

Bray, D.I. (1982). Regime equations for gravel-bed rivers. In: Gravel-Bed Rivers: Fluvial Processes, Engineering and Management, Hey, R.D., Bathurst, J.C., Thorne, C.R., Eds.,. John Wiley and Sons, Chichester, England, pp. 517 – 552

Callander, R. A. (1969), Instability and river channels, Journal of Fluid Mechanics, 36(03), 465-480, doi: 10.1017/S0022112069001765.

Carson, M. A., and G. A. Griffiths (1989), Gravel transport in the braided Waimakariri River: Mechanisms, measurements and predictions, Journal of Hydrology, 109(3–4), 201-220, doi: 10.1016/0022-1694(89)90016-4.

Colombini, M., G. Seminara, and M. Tubino (1987), Finite-amplitude alternate bars, Journal of Fluid Mechanics, 181, 213-232, doi: 10.1017/S0022112087002064.

Crosato, A., and E. Mosselman (2009), Simple physics-based predictor for the number of river bars and the transition between meandering and braiding, Water Resour. Res., 45(3), 1–14, doi:10.1029/2008WR007242.

Crosato, A., and M. S. Saleh (2011), Numerical study on the effects of floodplain vegetation on river planform style, Earth Surface Processes and Landforms, 36(6), 711-720, doi: 10.1002/esp.2088.

Crosato, A., E. Mosselman, F. Beidmariam Desta, and W. S. J. Uijttewaal (2011), Experimental and numerical evidence for intrinsic nonmigrating bars in alluvial channels, Water Resour. Res., 47(3), W03511, doi: 10.1029/2010WR009714.

Crosato, A., F. B. Desta, J. Cornelisse, F. Schuurman, and W. S. J. Uijttewaal (2012), Experimental and numerical findings on the long-term evolution of migrating alternate bars in alluvial channels, Water Resour. Res., 48(6), W06524, doi: 10.1029/2011WR011320.

Dinehart, R. L. (1992), Evolution of coarse gravel bed forms: Field measurements at flood stage, Water Resour. Res., 28(10), 2667-2689, doi: 10.1029/92WR01357.

Egozi, R., and P. Ashmore (2008), Defining and measuring braiding intensity, Earth Surface Processes and Landforms, 33(14), 2121-2138, doi:10.1002/esp.1658.

Engelund, F. (1970), Instability of erodible beds, Journal of Fluid Mechanics, 42(02), 225-244, doi: 10.1017/S0022112070001210.

Engelund, F., and O. Skovgaard (1973), On the origin of meandering and braiding in alluvial streams, Journal of Fluid Mechanics, 57(02), 289-302, doi: 10.1017/S0022112073001163.

Enggrob, H.G. and S. Tjerry (1999), Simulation of morphological characteristics of a braided river, in *Proceedings of the IAHR Symposium on River, Coastal and Estuarine Morphodynamics*, Genova, 6-10 Sept., Vol. I, 585-594.

FredsØe, J. (1978), Meandering and braiding of rivers, Journal of Fluid Mechanics, 84(04), 609-624, doi:10.1017/S0022112078000373.

Gaeuman, D., E. D. Andrews, A. Krause, and W. Smith (2009), Predicting fractional bed load transport rates: Application of the Wilcock-Crowe equations to a regulated gravel bed river, Water Resour. Res., 45(6), W06409, doi: 10.1029/2008WR007320.

Griffiths, G. A. (1979), Recent Sedimentation History of the Waimakariri River, New Zealand, Journal of Hydrology (New Zealand), 18 (I), 6-28.

Hey, D., and C.R. Thorne (1986), Stable channels with mobile gravel beds. Journal of Hydraulic Engineering, ASCE, Vol. 112, No. 8, pp. 671-689, doi: 10.1061/(ASCE)0733-9429(1986)112:8(671).

Hicks, D.M., M.J. Duncan, J.M. Walsh, R.M. Westaway, and S.N. Lane (2002), New views of the morphodynamics of large braided rivers from high-resolution topographic surveys and time-lapse video. In: *The structure, Function and management Implications of Fluvial Sedimentary Systems*, Proc. Int. Symp., Alice Springs, Australia, IAHS Publ. no. 276, 373-380.

Hicks, D.M., M.J. Duncan, S.N. Lane, M. Tal, and R.M. Westaway (2008), Contemporary morphological change in braided gravel-bed rivers: new developments from field and laboratory studies, with particular reference to the influence of riparian vegetation, in: Gravel-bed Rivers VI: From Process Understanding to River Restoration, H. Habersack, H. Piegay, M. Rinaldi, Eds., Elsevier, Chapter 21, 557-584.

Hirano M (1971) River bed degradation with armouring. Transactions of the Japanese Society of Civil Engineers 3: 194-195

Huang, H.Q. (2010), Reformulation of the bed load equation of Meyer and Peter and Müller in light of the linearity theory for alluvial channel flow, Water Res. Res. W09533, doi:10.1029/2009WR008974.

Hundey, E. J., and P. E. Ashmore (2009), Length scale of braided river morphology, Water Resour. Res., 45(8), n/a-n/a, doi:10.1029/2008WR007521.

Hunziker, R. P., and M. N. R. Jaeggi (2002), Grain Sorting Processes, Journal of Hydraulic Engineering, 128(12), 1060-1068, doi: 10.1061/(ASCE)0733-9429(2002)128:12(1060).

Jagers, H. R. A. (2003), Modelling planform changes of braided rivers. PhD thesis, Tewnte University, Enschede, the Netherlands. ISBN 90-9016879-6.

Jansen, PPh., L. van Bendegom, J. van den Berg, M. de Vries, A. Vanen (1979), Principles of River Engineering; the Non-Tidal Alluvial River, Pitman, London.

Kasprak, A., J. M. Wheaton, P. E. Ashmore, J. W. Hensleigh, and S. Peirce (2015), The relationship between particle travel distance and channel morphology: Results from physical models of braided rivers, J. Geophys. Res. Earth Surf., 120(1), 55–74, doi:10.1002/2014JF003310.

Kleinhans, M.G. and van den Berg, J.H. (2011), River channel and bar patterns explained and predicted by an empirical and a physics-based method. Earth Surface Processes and Landforms, 36, 721-738, doi: 10.1002/esp.2090.

Kleinhans, M. G., H. R. A. Jagers, E. Mosselman, and C. J. Sloff (2008), Bifurcation dynamics and avulsion duration in meandering rivers by one-dimensional and three dimensional models. Water Resources Research, 44, W08454, doi: 10.1029/2007WR005912.

Koch, F. G., and C. Flokstra (1980), Bed Level Computations for Curved Alluvial Channels, paper presented at XIXth congress of the International Association for Hydraulic Research, New Delhi, India,, 2-7 Feb. 1981.

Lane, E. W. (1957), A Study of the Shape of Channels Formed by Natural Streams Flowing in Erodible Material., edited, Missouri River Division Sediment Series No. 9. U.S. Army Engineer Division, Missouri River Corps of Engineers, Omaha, NE.

Lanzoni, S. (2000a), Experiments on bar formation in a straight flume: 1. Uniform sediment, Water Resour. Res., 36(11), 3337-3349, doi: 10.1029/2000WR900160.

Lanzoni, S. (2000b), Experiments on bar formation in a straight flume: 2. Graded sediment, Water Resour. Res., 36(11), 3351-3363, doi: 10.1029/2000WR900161.

Lanzoni, S., and M. Tubino (1999), Grain sorting and bar instability, Journal of Fluid Mechanics, 393, 149-174, doi: 10.1017/S0022112099005583.

Le Lay, Y. F., H. Piégay, and A. Rivière-Honegger (2013), Perception of braided river landscapes: Implications for public participation and sustainable management, J. Environ. Manage., 119, 1–12, doi:10.1016/j.jenvman.2013.01.006.

Leduc, P., P. Ashmore, and J. T. Gardner (2015), Grain sorting in the morphological active layer of a braided river physical model, Earth Surf. Dyn., 3(4), 577–585, doi:10.5194/esurf-3-577-2015.

Leopold, L. B., and M. G. Wolman (1957), River Channel Patterns: Braided, Meandering, and Straight, in Professional Paper, edited, pp. iv, p. 39-85, U.S. Geological Survey.

Lesser, G. R., J. A. Roelvink, J. A. T. M. van Kester, and G. S. Stelling (2004), Development and validation of a three-dimensional morphological model, Coastal Engineering, 51(8–9), 883-915, doi: 10.1016/j.coastaleng.2004.07.014.

Liébault, F., H. Piégay, P. Frey, and N. Landon (2008), Tributaries and the Management of Main-Stem Geomorphology, in River Confluences, Tributaries and the Fluvial Network, pp. 243–270, John Wiley & Sons, Ltd, Chichester, UK.

Marciano, R., Z. B. Wang, A. Hibma, H. J. de Vriend, and A. Defina (2005), Modeling of channel patterns in short tidal basins, J. Geophys. Res., 110(F1), F01001, doi: 10.1029/2003JF000092

Marra, W.A. (2008), Dynamics and interactions of bars in rivers and the relation between bars and a braided river pattern. B.S. Thesis, Faculty of Geosciences, Dep. of Physical Geography, Utrecht, Netherlands.

Mendoza, A., J. D. Abad, E. J. Langendoen, M. Asce, D. Wang, P. Tassi, K. El, and K. Abderrezzak (2003), Effect of Sediment Transport Boundary Conditions on the Numerical Modeling of Bed Morphodynamics, , 1–12, doi:10.1061/(ASCE)HY.1943-7900.0001208.

Meyer Peter, E., and R. Müller (1948), Formulas for bed load transport, in: Proc. of 2nd IAHR Congress, Stockholm, Sweden, edited, pp. 39-64.

Miall, A. D. (1977), A review of the braided-river depositional environment, Earth-Science Rev., 13(1), 1–62, doi:10.1016/0012-8252(77)90055-1.

Mosselman, E. (2005), Basic Equations for Sediment Transport in CFD for Fluvial Morphodynamics, in Computational Fluid Dynamics, edited, pp. 71-89, John Wiley & Sons, Ltd., doi: 10.1002/0470015195.ch4.

Mosselman, E. and Le, T.B. (2015). Five common mistakes in fluvial morphodynamic modelling. *Advances in Water Resources*, doi: 10.1016/j.advwatres.2015.07.025.

Nicholas, A.P. (2000), Modelling bedload yield in braided gravel bed rivers, Geomorphology, 36(1–2), 89-106, doi: 10.1016/S0169-555X(00)00050-7.

Nicholas, A.P. (2013), Modelling the continuum of river channel patterns, Earth Surface Processes and Landforms, 38, 1187-1196, doi: 10.1002/esp.3431.

Nicholas, a. P., P. J. Ashworth, G. H. Sambrook Smith, and S. D. Sandbach (2013), Numerical simulation of bar and island morphodynamics in anabranching megarivers, J. Geophys. Res. Earth Surf., 118(4), 2019–2044, doi:10.1002/jgrf.20132.

Parker, G. (1976), On the cause and characteristic scales of meandering and braiding in rivers, Journal of Fluid Mechanics, 76(03), 457-480, doi: 10.1017/S0022112076000748.

Parker, G. (1991), Selective Sorting and Abrasion of River Gravel. I: Theory, Journal of Hydraulic Engineering, 117(2), 131-147, doi: 10.1061/(ASCE)0733-9429(1991)117:2(131).

Parker, G. (2007), Transport of gravel and sediment mixtures, in: Sedimentation Engineering: Theories, Measurements, Modeling and Practice, ASCE Manual Rep. Eng. Practice,Vol.110, edited by M.H. Garcia, Chapter 3, pp. 165–264, doi: 10.1061/9780784408148.ch03.

Parker, G., P. C. Klingeman, and D. G. Mc Lean (1982), Bedload and size distribution in paved gravel-bed streams. Journal of the Hydraulic Division, ASCE, 108, HY4, 544-571.

Parker, G., P. R. Wilcock, C. Paola, W. E. Dietrich, and J. Pitlick (2007), Physical basis for quasi-universal relations describing bankfull hydraulic geometry of single-thread gravel bed rivers, J. Geophys. Res., 112(F4), F04005, doi: 10.1029/2006JF000549.

Peters, J. J. (1978), Discharge and sand transport in the braided zone of the Zaire estuary, Netherlands Journal of Sea Research, 12(3-4), 273-292.

Pigay, H., G. Grant, F. Nakamura, and N. Trustrum (2006), Braided River Management: from Assessment of River Behaviour to Improved Sustainable Development, in Braided Rivers, pp. 257–275, Blackwell Publishing Ltd., Oxford, UK.

Piégay, H., A. Alber, L. Slater, and L. Bourdin (2009), Census and typology of braided rivers in the French Alps, Aquat. Sci., 71(3), 371–388, doi:10.1007/s00027-009-9220-4.

Powell, D. M. (1998), Patterns and processes of sediment sorting in gravel-bed rivers, Progress in Physical Geography, 22(1), 1-32, doi: 10.1177/030913339802200101.

Ribberink, J. S. (1987), Mathematical modelling of one-dimensional morphological changes in rivers with non-uniform sediment, Phd Thesis, Delft University of Technology, Delft, The Netherlands.

Rinaldi, M., C. Simoncini, and H. Piégay (2009), Scientific design strategy for promoting sustainable sediment management: the case of the Magra River (Central-Northern Italy), *River Res. Appl.*, *25*(5), 607–625, doi:10.1002/rra.1243.

Roelvink, J. A. (2006), Coastal morphodynamic evolution techniques, Coastal Engineering, 53(2–3), 277-287, doi: 10.1016/j.coastaleng.2005.10.015.

Rust, B. R. (1972), Structure and process in a braided river, Sedimentology, 18(3–4), 221–245, doi:10.1111/j.1365-3091.1972.tb00013.x.

Sadler, J. P., D. Bell, and A. Fowles (2004), The hydroecological controls and conservation value of beetles on exposed riverine sediments in England and Wales, Biol. Conserv., 118(1), 41–56, doi:10.1016/j.biocon.2003.07.007.

Schielen, R., A. Doelman, and H. E. de Swart (1993), On the non-linear dynamics of free bars in straight channels, Journal of Fluid Mechanics, 252, 325-356, doi: 10.1017/S0022112093003787.

Schuurman, F., and M. G. Kleinhans (2011), Self-formed braided bar pattern in a numerical model, in Proceedings River, Coastal and Estuarine Morphodynamics, edited, pp. 1647-1657, Tsinghua University Press.

Schuurman, F., Marra, W. A. and M. G. Kleinhans (2013), Physics-based modeling of large braided sand-bed rivers: bar pattern formation, dynamics and sensitivity. J of Geophys. Research: Earth Surface, 118, 2509-2527, doi: 10.1002/2013JF002896.

Seminara, G., and M. Tubino (1989), Alternate bars and meandering: Free, forced and mixed interactions, in River Meandering, Water Resour. Monogr. Ser., vol. 12, edited by S. Ikeda and G. Parker, pp. 267–320, AGU, Washington, D. C., doi:10.1029/WM012p0267.

Siviglia, A., and A. Crosato (2016), Numerical modelling of river morphodynamics: latest developments and remaining challenges, Adv. Water Resour., doi:10.1016/j.advwatres.2016.01.005

Sloff, C. J., and W. Ottevanger (2008), Multiple-layer graded-sediment approach: improvement and implications, in River Flow 2008, Taylor and Francis/Balkema. Proceedings, edited by K. Altinakar, Gogus, Tayfur, Kumcu & Yildirim, pp. 1447-1456.

Sloff, C. J., Jagers, H. R. A., Kitamura, Y and P. Kitamura (2001), 2D Morphodynamic modelling with graded sediment, in In: Proc. of 2nd IAHR Symp. on River, Coastal and Eastuarine Morphodynamics 10-14 sept, 2001, Obiro, Japan, edited.

Sloff, K. and E. Mosselman (2012), Bifurcation modelling in a meandering gravel-sand bed river. Earth Surf. Process. Landforms 37, 1556-1566, doi: 10.1002/esp.3305.

Sun, J., B. Lin, and H. Yang (2015), Development and application of a braided river model with non-uniform sediment transport, Adv. Water Resour., doi:10.1016/j.advwatres.2014.12.012.

Surian, N., and M. Rinaldi (2003), Morphological response to river engineering and management in alluvial channels in Italy, Geomorphology, 50(4), 307–326, doi:10.1016/S0169-555X(02)00219-2.

Surian, N., L. Mao, M. Giacomin, and L. Ziliani (2009), Morphological effects of different channel-forming discharges in a gravel-bed river, Earth Surf. Process. Landforms, 1107(March), 1093–1107, doi:10.1002/esp.

Talmon, A. M., N. Struiksma, and M. C. L. M. Van Mierlo (1995), Laboratory measurements of the direction of sediment transport on transverse alluvial-bed slopes, Journal of Hydraulic Research, 33(4), 495-517, doi: 10.1080/00221689509498657.

Teramoto, A., and T. Tsujimoto (2006), Effects of size heterogeneity of bed materials on mechanism to determine bar mode, in: River, Coastal and Estuarine Morphodynamics RCEM 2005, edited by G. Parker and M. Garcia, Taylor & Francis, pp. 433-444.

Tockner, K., F. Malard, and J. V. Ward (2000), An extension of the flood pulse concept, Hydrol. Process., 14(16–17), 2861–2883, doi:10.1002/1099-1085(200011/12)14:16/17<2861::AID-HYP124>3.0.CO;2-F.

Tockner, K., A. Paetzold, U. Karaus, C. Claret, and J. Zettel (2006), Ecology of Braided Rivers, in Braided Rivers, pp. 339–359, Blackwell Publishing Ltd., Oxford, UK.

van den Berg, J. H. (1995), Prediction of alluvial channel pattern of perennial rivers, Geomorphology, 12(4), 259-279, doi: 10.1016/0169-555X(95)00014-V.

van der Nat, D., K. Tockner, P. J. Edwards, J. V. Ward, and A. M. Gurnell (2003), Habitat change in braided flood plains (Tagliamento, NE-Italy), Freshw. Biol., 48(10), 1799–1812, doi:10.1046/j.1365-2427.2003.01126.x.

van der Wegen M. and J.A. Roelvink (2008), Long-term morphodynamic evolution of a tidal embayment using a two-dimensional, process-based model. J. Geophys. Res., 113, C03016, doi: 10.1029/2006JC003983.

Wang, Z. B., M. C. J. L. Jeuken, H. Gerritsen, H. J. de Vriend, and B. A. Kornman (2002), Morphology and asymmetry of the vertical tide in the Westerschelde estuary, Continental Shelf Research, 22(17), 2599-2609, doi: 10.1016/S0278-4343(02)00134-6.

Wilcock, P. R., and J. C. Crowe (2003), Surface-based Transport Model for Mixed-Size Sediment, Journal of Hydraulic Engineering, 129(2), 120-128, doi: 10.1061/(ASCE)0733-9429(2003)129:2(120).

Willgoose, G., and G. Hancock (1998), Revisiting the hypsometric curve as an indicator of form and process in transport-limited catchment, Earth Surface Processes and Landforms, 23(7), 611-623, doi: 10.1002/(SICI)1096-9837(199807)23:7<611::AID-ESP872>3.0.CO;2-Y.

Wong, M., and G. Parker (2006), Reanalysis and Correction of Bed-Load Relation of Meyer Peter and Müller Using Their Own Database, Journal of Hydraulic Engineering, 132(11), 1159-1168, doi: 10.1061/(ASCE)0733-9429(2006)132:11(1159).

Wu, W., Shields, F.D. Jr., Bennet, S.J. and S.S.Y. Wang (2005), A depth averaged two dimensional model for flow, sediment transport, and bed topography in curved channels with riparian vegetation. Water Resour. Res., 41, W03015, doi:10.1029/2004WR003730.

Yossef, M.F.M. and K. Sloff (2012), Detailed Modelling of River Morphological Response to Climate Change Scenarios. River Flow 2012, Murillo Munoz R.E. ed., CRC Press/Balkema, Leiden, the Netherlands, Volume 1, 845-852.